

# The sintering mechanism of fully dense and highly coercive Nd-Fe-B magnets from the recycled HDDR powders reprocessed by Spark Plasma Sintering.

Awais Ikram<sup>1,2,\*</sup>, M. Farhan Mehmood<sup>1,2</sup>, Mateja Podlogar<sup>1</sup>, Anas Eldosouky<sup>2,4</sup>, Richard Stuart Sheridan<sup>3</sup>, Muhammad Awais<sup>3</sup>, Allan Walton<sup>3</sup>, Marjeta Maček Kržmanc<sup>5</sup>, Tomaz Tomse<sup>1,2</sup>, Spomenka Kobe<sup>1,2</sup>, Saso Sturm<sup>1,2</sup>, Kristina Zuzek Rozman<sup>1,2</sup>.

<sup>1</sup>Department for Nanostructured Materials, Jožef Stefan Institute, Jamova cesta 39, SI-1000 Ljubljana, Slovenia,

<sup>2</sup>Jožef Stefan International Postgraduate School, Jamova cesta 39, SI-1000 Ljubljana, Slovenia,

<sup>3</sup>School of Metallurgy and Materials, University of Birmingham, Edgbaston, Birmingham, B15 2TT, United Kingdom

<sup>4</sup>Magneti Ljubljana, d.d., Stegne 37, SI-1000 Ljubljana, Slovenia.

<sup>5</sup>Advanced Materials Department, Jožef Stefan Institute, Jamova cesta 39, Ljubljana 1000, Slovenia.

## Abstract

The goal of this study was to justify the reprocessing of recycled HDDR Nd-Fe-B powders with spark plasma sintering (SPS) and to investigate the dependence of the final magnetic properties on SPS and thermal treatment. The initial recycled HDDR powder of the composition  $\text{Nd}_{13.4}\text{Dy}_{0.6}\text{Fe}_{78.6}\text{B}_{6.1}\text{Nb}_{0.4}\text{Al}_{0.7}$  with 4760 ppm  $\text{O}_2$  content, coercivity ( $H_{\text{Ci}}$ ) = 830 kA/m, and large particle size distribution <50 – 600  $\mu\text{m}$ , was treated using the SPS parameters as follows:  $T = 650 - 850$  °C for 1 – 5 minutes and 50 MPa pressure. The post SPS thermal treatment was performed at 750 °C for 15 minutes in vacuum. The optimal SPS conditions at 750 °C for 1 min, yielded fully dense magnets with the coercivity  $H_{\text{Ci}} = 1060$  kA/m, which was boosted to 1160 kA/m after the post-SPS thermal treatment. The grain growth was obvious in samples SPS-ed above 800 °C and subsequently, the  $H_{\text{Ci}}$  was reduced. The SPS reprocessing beyond 850 °C was found to be detrimental to the overall magnetic properties due to the formation of bimodal grain size distribution origination from the abnormal grain growth (700 – 2600 nm). The redistribution of Nd-rich grain boundary phase between the  $\text{Nd}_2\text{Fe}_{14}\text{B}$  matrix grains in thermally treated magnets and the relaxation of the internal stresses induced via SPS are the possible reasons for the  $H_{\text{Ci}}$  surpassing the  $H_{\text{Ci}}$  of the starting recycled HDDR powder. It was shown that the SPS consolidation technique is suitable for producing fully dense nanograined bulk Nd-Fe-B magnets, with coercivities even exceeding the initial HDDR-powder and is one of the most suitable routes for revitalizing the Nd-Fe-B scrap magnets.

**Keywords:** Rare Earth, Permanent Magnets,  $\text{Nd}_2\text{Fe}_{14}\text{B}$ , Recycling, Spark Plasma Sintering, Reprocessing, Coercivity, HDDR, HD, Nanocrystalline.

## 1. Introduction

Since the discovery of the rare-earth-based Nd-Fe-B type permanent magnets in 1984 [1, 2], they became essential in energy, telecommunication, microelectronics and aerospace applications, as well in medical equipment, computers, sensors, electric motors and fusion devices [3 - 5]. However, in 2011, the rare earth elements (REE)

\* Corresponding Author.

Email: [awais.ikram@ijs.si](mailto:awais.ikram@ijs.si) (Awais Ikram)

importers met a supply chain crisis and as a result, the prices soared [6]. Since the REE are a backbone for the green technologies, the EU now considers them as the most critical raw materials in terms of supply risk [6]. In comparison with the light rare earth elements (LREE), the heavy rare earth elements (HREE) like Dy, Tb, Ho etc. are more scarce and hence, more expensive. Dy is consistently used as a dopant to increase coercivity in high-performance permanent magnets, suitable for applications above 100 °C [4, 6]. This, however, decreases the remanence ( $B_r$ ) and the  $BH_{max}$ , due to the antiferromagnetic coupling of Dy with Fe atoms. Increasing the coercivity ( $H_{ci}$ ) of Nd-Fe-B magnets without the HREE addition can be done via grain boundary modification treatments, which increases the grain boundary phase thickness in a way that neighboring grains become magnetically decoupled [4]. The other option is to develop near single domain nanostructured  $Nd_2Fe_{14}B$  grains ( $\leq 400$  nm). This can be achieved via melt spinning or by utilizing the Hydrogenation-Disproportionation-Desorption-Recombination (HDDR) process [5]. The grain size refinement is considered a very viable option as it enhances the  $H_{ci}$  [4] without HREE addition. However, such nanograined powder cannot be manufactured via the conventional sintering route, as the  $Nd_2Fe_{14}B$  grains will grow exponentially with temperature exceeding 1000 °C and the  $H_{ci}$  will be lost [4, 5], therefore alternative processing routes have to be proposed.

In view of the REE crisis and knowing that the industrial processing wastes in permanent magnet production accounts to  $\geq 25\%$  for REE [7, 8] it became feasible to recycle and reprocess them. The end-of-life (EOL) permanent magnets can be recycled using the hydrogen decrepitation process [8] to form non-magnetic powders, which can further be reprocessed and reused as suggested by Li Xiantao et al. [7]. Several researchers [7–19] have reported with varying degree of success on recycling the scrap Nd-Fe-B and reprocessing by conventional sintering of hydrogen decrepitated (HD) and jet-milled recycled powder [8, 9]. However, to date, no trials have been made on the sintered magnets from recycled HDDR powders and only low  $H_{ci}$  bonded magnets have been reported [7]. The HDDR reprocessing has been utilized in recycling by Walton et al. [9] and Sheridan et al. [13] to make nanocrystalline powders, but for bonded magnet applications only. However, the reports from McGuinness [20] and Mueller [21] on Zr-doped hot pressed HDDR powders indicate that fully dense magnets can be processed without a significant loss in the  $H_{ci}$  compared to the starting powder. It is evident that the rapid compaction techniques e.g. shock compaction can be used in the alternate strategy to develop nanocrystalline bulk sintered Nd-Fe-B magnets without degrading their  $H_{ci}$  [5]. The Spark Plasma Sintering (SPS) compaction method would represent a suitable alternative to produce dense magnets. The SPS-ed fresh and commercial grade HDDR Nd-Fe-B powder was already processed by Suresh et al. [22] and Takagi et al. [23], which have indicated the possibility to fully densify the HDDR powders within a few minutes at 600 - 750 °C. These corresponding SPS temperatures are 30 – 40 % lower than the ones used in conventional vacuum sintering ( $> 1050$  °C). However, after SPS-ing the  $H_{ci}$  was lost and only regained subsequently by post-sinter annealing treatments, attributed to the redistribution of the Nd-rich grain boundary phase and the intergrain stress relaxation [22 – 26]. The reason for this overall low  $H_{ci}$  in compacted samples having near single domain structure has been attributed to inadequate grain isolation, by only a thin paramagnetic Nd-rich grain boundary phase, identified previously by Gopalan et al. [24] and Li et al. [25]. To achieve adequate localized grain

\* Corresponding Author.

Email: [awais.ikram@ijs.si](mailto:awais.ikram@ijs.si) (Awais Ikram)

73 decoupling, enough paramagnetic Nd-rich phase must be uniformly distributed between the matrix grains and for  
74 this reason, the excess Nd is added to the composition to compensate for the Nd-loss due to oxidation during the  
75 recycling process [4, 10, 15]. With the focus of increasing the  $BH_{max}$ , tackling the remnant magnetization is also one  
76 of the major factors, however, compacted HDDR powders express usually low remanence ( $B_r$ ) which is reasoned to a  
77 poor degree of easy axis alignment (texture) after compaction [24]. The mechanism for microstructure development  
78 in the HDDR powder consolidated with the SPS is still to be determined, and only then the SPS parameters and  
79 resultant microstructure can be controlled for maximizing the  $H_{Ci}$  of near single domain grained HDDR powder.

80  
81 Our study proposes the reprocessing of HDDR powders from EOL magnetic scrap using the SPS process for the first  
82 time, to contribute to the already existing state-of-the-art of the nanocrystalline HDDR Nd-Fe-B powders. The EOL  
83 scrap magnet HDDR powder in comparison to the “fresh/commercial” HDDR powder has a higher overall oxygen  
84 content, therefore obtaining high  $H_{Ci}$  presents a challenge with such Nd-Fe-B system. As K. Takagi et al [23] reported  
85 that the particle size distribution is crucial in determining the  $H_{Ci}$  of SPS-ed HDDR powder, as different HDDR particle  
86 fractions were associated with the different degree of surface oxidation, leading to lower  $H_{Ci}$  for smaller particles.  
87 However, to date, the  $H_{Ci}$  decrease due to oxidation has not been yet fully understood in terms of the  
88 microstructure [23, 27, 28]. Unlike commercial or fresh SPS-ed HDDR powder in which the  $H_{Ci}$  drops after SPS and  
89 the properties have to be recovered with proper annealing treatment [23], we have demonstrated that a direct SPS  
90 reprocessing of the recycled HDDR powders with near stoichiometric composition, does result in even higher  $H_{Ci}$   
91 than the starting HDDR powder. The combination of rapid high-temperature SPS and thermal treatment above the  
92 eutectic temperature allowed us to preserve the grains from growing, achieving full densification and redistributing  
93 the Nd-rich grain boundary phase, diminishing the intergranular stresses and increasing the  $H_{Ci}$ . This research work  
94 approves the application of SPS for developing nanostructured sintered magnets, even from the recycled HDDR Nd-  
95 Fe-B powders.

## 96 2. Experimental

97 The original end-of-life (EOL) sintered Nd-Fe-B magnets had  $H_{Ci} = 1170$  kA/m and  $B_r = 1.19$  T. These EOL magnets  
98 were HD treated and pulverized to reduce particle size. Further, these particles were HDDR reprocessed; complete  
99 details of this process has been previously reported by Sheridan et al. [13, 29] for producing the anisotropic recycled  
100 powder. The EOL scrap magnet has an overall oxygen content of 2660 ppm (0.266 wt. %). After the HDDR process,  
101 the oxygen content increased to 4760 ppm (0.476 wt. %). The intrinsic magnetic properties of recycled HDDR  
102 powder were measured as a bonded magnet with the Lakeshore VSM (not adjusting for self-demagnetization). The  
103 measured  $J_s$  value accounts to 1.4 T. The EOL sintered magnets having a nominal composition of  
104  $Nd_{13.4}Dy_{0.6}Fe_{78.6}B_{6.1}Nb_{0.4}Al_{0.7}$  measured with Inductively Coupled Plasma Mass Spectroscopy (ICP-MS) were HD treated  
105 and then the dynamic hydrogenation-disproportionation-desorption-recombination (d-HDDR) process was utilized to  
106 develop recycled powder with nanostructured anisotropic grains. Detailed description of HDDR processing is  
107 provided by Sheridan et al. [13]. The theoretical density was calculated by measuring the weight fraction of the

\* Corresponding Author.

Email: [awais.ikram@ijs.si](mailto:awais.ikram@ijs.si) (Awais Ikram)

108 individual elements with the respective density of each element in the HDDR powder composition and it was  
109 approximated to  $7.57 \pm 0.01 \text{ g/cm}^3$ . This recycled HDDR powder had a wide particle size distribution as measured  
110 from HR-SEM. The phase analysis for the recycled HDDR powder was performed using the XRD (PANalytical  
111 Empyrean Diffractometer).

112  
113 The Curie temperature ( $T_C$ ), endothermic eutectic melting and exothermic crystallization processes were determined  
114 by Thermogravimetric Differential Scanning Calorimetry (TG-DSC) in the temperature range of 30 – 900 °C with the  
115 heating and cooling rates of 20 °C/min, under argon environment (99.99% purity, flow rate 50 ml/min.) using Jupiter  
116 449 Simultaneous Thermal Analysis (STA) instrument with TG-DSC-cp sample holder and Pt-crucibles with  $\text{Al}_2\text{O}_3$   
117 liners. The temperature and sensitivity calibration of the instrument was performed with In, Bi, Zn, Al and Au  
118 standards. Before the DSC analysis, the samples were exposed to air atmosphere only for a few minutes during  
119 weighing before repeated vacuuming ( $5 \times 10^{-4}$  mbar) and purging with Argon. The oxygen content of the HDDR  
120 powder and particle fractions was measured by Eltra ON 900, oxygen and nitrogen analyzer. In order to estimate the  
121 average particle size, the sieving of HDDR powder was performed from 1 mm sieve down to < 50  $\mu\text{m}$  sieve size in a  
122 glove box to prevent any oxidation of the recycled powder before the XRD, the microstructural characterization and  
123 the SPS reprocessing.

124  
125 For the preparation of the SPS sintered magnets out of the recycled HDDR powder, the cylindrical graphite dies of 16  
126 mm internal diameter were used and 5 g of the recycled HDDR powder was added in between the graphite foils and  
127 spacers. Punches were placed in to squeeze the powder compactly. Further pre-pressing or magnetic pre-alignment  
128 of the HDDR powders in the graphite molds was not performed before sintering for making isotropic magnets. These  
129 prepared molds were then placed in Syntex 3000 (DR. SINTER) SPS furnace with controlled pressure unit and a  
130 thermocouple. All the SPS experiments were performed under a vacuum of  $2 \times 10^{-2}$  mbar and a constant uniaxial  
131 pressure of 50 MPa was maintained. The sintering temperature was varied from 650 – 850 °C, with a heating ramp  
132 of 50 °C/minute. The holding time at the sintering temperature was kept from 1 – 5 minute (s). The SPS temperature  
133 was controlled with a calibrated thermocouple. All the SPS-ed samples were grinded using 500 grit size SiC papers to  
134 peel off the graphite spacers. Fine grinding up to 4000 grit was done further and the samples were polished on  
135 rotary disks using 1/4  $\mu\text{m}$  diamond paste on the velvet cloth. Samples were then analyzed for the magnetic  
136 properties on a permeameter (Magnet-Physik Dr. Steingroever) by taking successive magnetization and  
137 demagnetization measurements. The density measurements were taken on density-meter (DENSITEC) utilizing the  
138 Archimedean principle and immersed in silicone oil.

139  
140 Post-sinter thermal treatments (PST) were performed under a vacuum of  $> 10^{-5}$  mbar at a heating rate of 50  
141 °C/minute in a horizontal tube furnace. The isothermal annealing temperature was kept at 750 °C and the samples  
142 were held for 15 minutes at this temperature. The density and magnetic measurements were repeated after the  
143 annealing step. For the microstructural investigations SPS-ed and post thermally treated samples etched with 3M  
144 Cyphos. The microstructural investigation was performed on the recycled etched and non-etched HDDR powder, the  
\* Corresponding Author.

Email: [awais.ikram@ijs.si](mailto:awais.ikram@ijs.si) (Awais Ikram)

145 SPS-ed and the PST specimens using Field Emission Scanning Electron Microscope (JEOL 7600F and FEI Helios  
146 NanoLab DualBeam 650 FIB with Oxford Aztec 50 mm<sup>2</sup>). Electron energy dispersive X-ray spectroscopy (EDS) was  
147 performed at 20 keV.

\* Corresponding Author.

Email: [awais.ikram@ijs.si](mailto:awais.ikram@ijs.si) (Awais Ikram)

### 3. Results and Discussion

#### 3.1 Chemical, thermal, magnetic and crystal structure characterization of the recycled HDDR powder

In order to investigate the thermal behaviour of the starting HDDR powder to determine the SPS regime, thermal analysis was performed. Figure 1 (a) illustrates the typical TG and DSC curves obtained for recycled HDDR powder during heating at a heating rate of 20 °C/min to 900 °C peak temperature. The increase of mass due to oxidation during thermal analysis experiment was not significant (0.23%) and as it is very small and continuous (500 – 900 °C), its contribution to thermal effects could be neglected. DSC heating curve in Fig. 1 (a) is characterized by several endothermic effects. The low-temperature DSC peak, which was noticed at 307 °C, belongs to the Curie temperature ( $T_C$ ) of the Nd-Fe-B. The onset of  $T_C$  begins close to 260 °C. The enthalpy associated with this phase transition was 4.9 J/g, which is significant for this transition after several repeated experiments. Further on, the most intense DSC peak is observed at 743 °C with its transformation on-set at 665 °C. This DSC peak is very close to the already reported ternary eutectic temperature  $T_{ELM}$  (690 °C), where  $Nd_2Fe_{14}B$  matrix phase is present with liquefied  $\alpha$ -Nd [39], however slightly lower on-set temperature (665 °C) observed for HDDR powder in this study could be related to the presence of other elements such as Dy, Nb and Al in very low quantity, which might lower this eutectic temperature. Similarly, Vial et al. [42] also determined the eutectic temperature lower than 690 °C (646 °C) for the composition  $Nd_{12.4}Pr_{1.4}B_{5.8}Al_{0.3}Cu_{0.1}Fe_{79.9}$ , which was very similar to the material used in this work. In the DSC curve of this alloy with a minor content of Al, Cu and Co an additional endothermic peak was also noticed at 527 °C by the authors [42]. This peak could originate from Co and Cu containing compounds with a low melting temperature. Although Co and Cu are not constituents of the HDDR powder in the present study, a weak endothermic peak was observed in the lower temperature range at 477 °C. The measured enthalpy (0.6 J/g) associated with this low-temperature melting was considerably smaller than the characteristic (6.7 J/g) determined for the melting at higher temperature eutectic transformation between 665 °C and 770 °C. The formation of a low-temperature endothermic reaction in both systems containing Al implies that this melting is perhaps related to Al and its interactions in the system with Dy and Nd at the grain boundary interface. The enhanced melting effect of the grain boundary phase due to the presence of Al and Ni was already reported by N. Oono et al. [32].

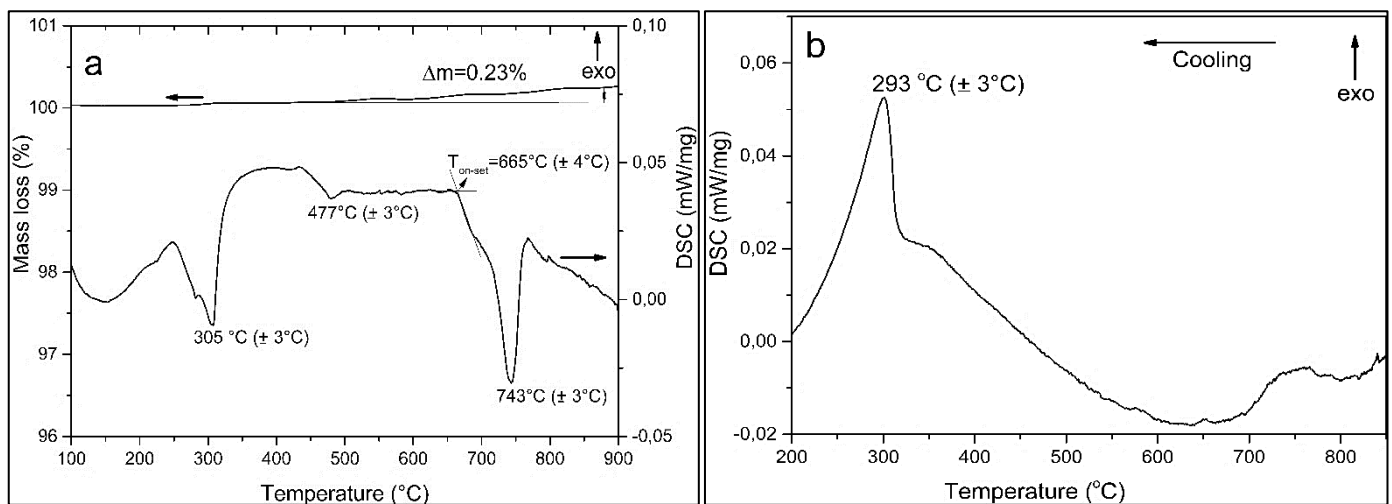


Figure 1: TG and DSC curves of (a) the recycled HDDR Nd-Fe-B powder during (a) heating and (b) cooling.

\* Corresponding Author.

Email: [awais.ikram@ijs.si](mailto:awais.ikram@ijs.si) (Awais Ikram)

175

176 In the cooling DSC curves of the HDDR powder, the exothermic peak belonging to the paramagnetic to ferromagnetic  
177 phase transition is well defined (Figure 1b). The onset begins close to 310 °C and the peak corresponds to  $T_c = 293$  °C  
178 for HDDR powder, so the results match during heating and cooling runs. The cooling DSC curve of HDDR powder was  
179 additionally characterized by weak and broad exothermic peak extending from 760 °C to 700 °C, which could be  
180 ascribed to the crystallization of the Nd-rich grain boundary phase. Since this process was associated with a rather  
181 small change of enthalpy (0.7 J/g) we can assume that during cooling with the rate of 20 °C/min the majority of grain  
182 boundary phase may possibly end up amorphous instead of well-defined crystalline grain boundaries due to the  
183 absence of well-defined peak(s). DSC measurements of the recycled HDDR powder samples were performed several  
184 times and very reproducible results were obtained. The initial Dy and Al additions to bulk magnets are reasoned to  
185 reduce this grain boundary phase melting temperature [32, 33, 39]. Therefore, the SPS reprocessing temperatures  
186 were kept in the 650 – 850 °C range to correlate the effect of the temperature to the microstructural evolution and  
187 its result on the magnetic properties, which will be discussed later. These measured values of  $T_c$  and  $T_{ELM}$  are  
188 synonymous with the work done by Hono et al. [39] on Nd-Fe-B.

189

190 The XRD analysis of the HDDR recycled powder is shown in Figure 2. The reflections correspond to the tetragonal  
191  $Nd_2Fe_{14}B$  hard magnetic phase with JCPDA reference numbers 00-036-1296 and 04-006-2691 as the major phase.  
192 The lattice parameters of matrix phase are:  $a = 8.79$  (Å),  $b = 8.79$  (Å) and  $c = 12.2$  (Å), with P42/mnm space group and  
193 space group number of 136. As the scrap magnet contained 0.6 at. % Dy, the  $DyNdFe_{14}B$  phase (JCPDA # 01-089-  
194 3548) with multiple overlapping peaks can be adjusted with the similar lattice parameters:  $a = 8.79$  (Å),  $b = 8.79$  (Å),  
195  $c = 12.1$  (Å) and P42/mnm space group. The Nd-oxide phases were also detected by XRD, attributing to the pickup of  
196 oxygen before and/or during the HDDR reprocessing. The cubic  $NdO_2$  (JCPDA # 04-007-0500) and  $Nd_2O_3$  (JCPDA # 00-  
197 040-1283) phases were detected. In addition, the  $NdFe_4B_4$  (JCPDA # 01-081-3530) phase was also present in the  
198 recycled HDDR powder which was to be expected.

\* Corresponding Author.

Email: [awais.ikram@ijs.si](mailto:awais.ikram@ijs.si) (Awais Ikram)

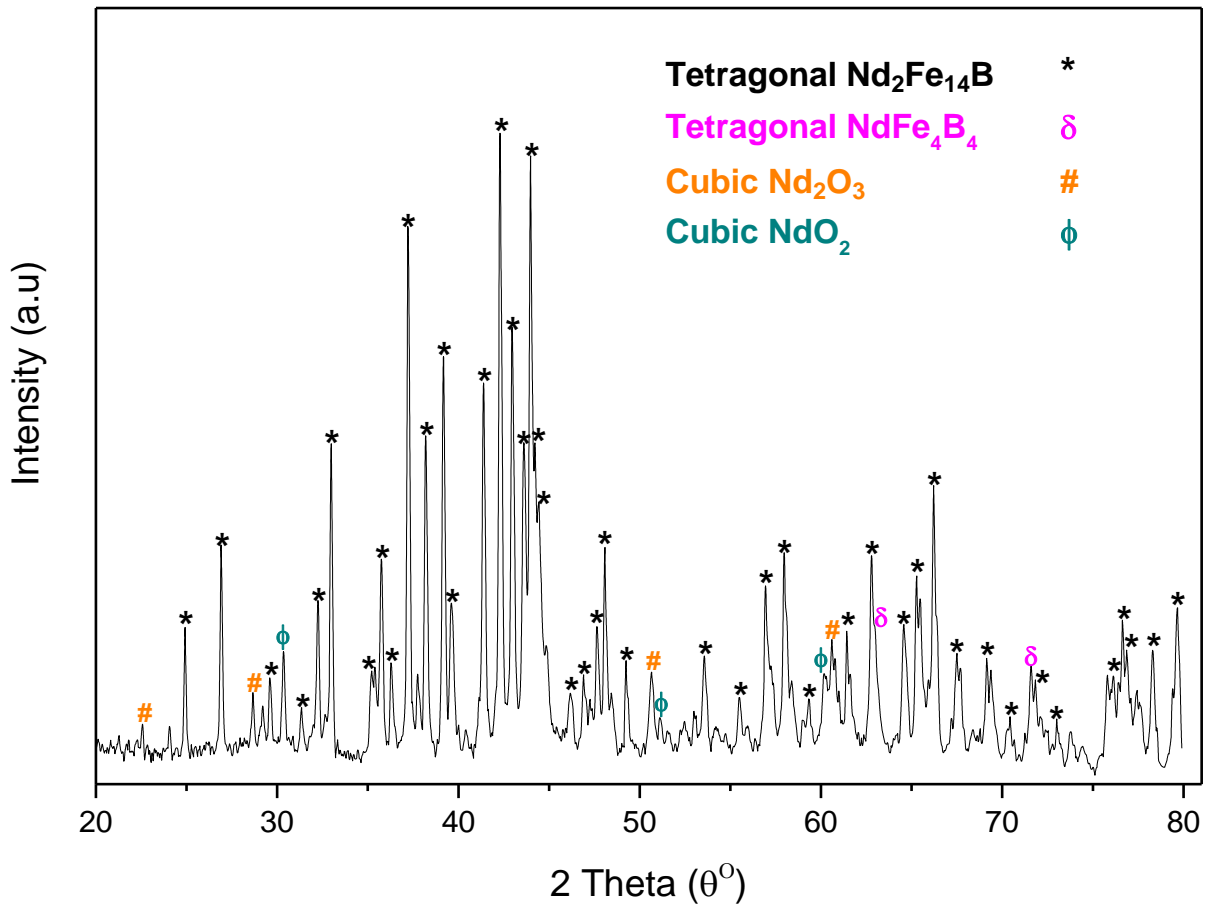


Figure 2 illustrates the XRD analysis of recycled HDDR powder.

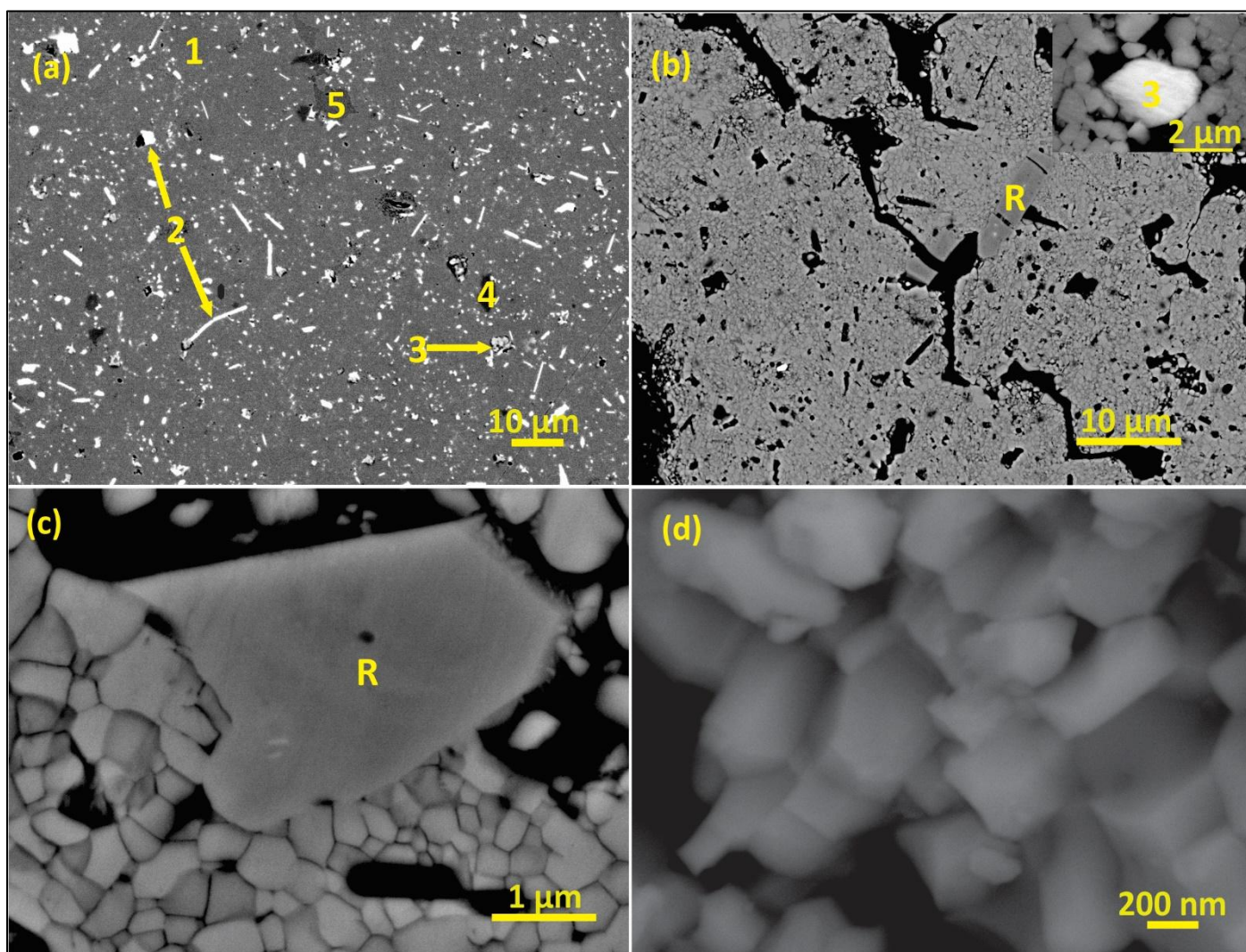
### 3.2 Characterization of the recycled HDDR powders.

Figure 3 shows the BSE SEM micrographs of polished recycled HDDR Nd-Fe-B powder prepared in epoxy resin. The particles have irregular shapes and a large particle size distribution, from 30 – 700  $\mu\text{m}$ , with an average particle size of 220  $\mu\text{m}$ . Figure 3 (a) shows a typical microstructure of the HDDR powder whereby the grey matrix corresponds to  $\text{Nd}_2\text{Fe}_{14}\text{B}$  (highlighted as 1) and the bright phases are Nd-rich intergranular phases,  $\text{NdO}_x$  (highlighted as 2) and  $\text{Nd}_2\text{O}_3$  (highlighted as 3) phases randomly scattered in the matrix. The EDS quantification of these phases is shown in Table 1. The darker contrast phases marked with “B” and “L” corresponding to  $\text{NdFe}_4\text{B}_4$  type borides and  $\text{NbFe}_2$  types Laves phases respectively. The Nb-rich phases are traced back from the EOL sintered scrap magnet forming  $\text{NbFe}_2$  type Laves phases scattered in the Nd-Fe-B matrix which are nonetheless not significant in volume to be traced with the XRD analysis of the recycled HDDR powder. The Nb addition in sintered magnets also improves  $H_{\text{Ci}}$  such that the grains of a hard phase become more regular and the interfaces with grain boundaries get wider and smoother [30]. Nb reportedly forms  $\text{NbFe}_2$  Laves phase during the recombination reaction, such that precipitation of  $\alpha\text{-Fe}$  is suppressed, as  $\alpha\text{-Fe}$  is known to substantially reduce the  $H_{\text{Ci}}$  [30, 31]. The Laves phase reappears in the recycled HDDR powder as quantified in EDS results in Table 1 and therefore no free bcc iron ( $\alpha\text{-Fe}$ ) was detected with either EDS or XRD. The other dark grey phase corresponds to the conversion of the boride phase from  $\text{Fe}_2\text{B}$  phase to

\* Corresponding Author.

Email: [awais.ikram@ijs.si](mailto:awais.ikram@ijs.si) (Awais Ikram)

217  $\text{NdFe}_4\text{B}_4$  type phase after the HDDR reaction [52]. SEM-EDS cannot accurately quantify boron, but Nd:Fe ratio of 1:4  
 218 was detected from this phase as shown in Table 1.



219  
 220 Figure 3 : HR-SEM BSE images of the initial recycled HDDR powder, (a) "1"  $\text{Nd}_2\text{Fe}_{14}\text{B}$  matrix phase, "2" the bright Nd-rich grain  
 221 boundary phase, "3" the Nd-oxide phase, "4" is Nb-Fe Laves phase and "5" are the  $\text{NdFe}_4\text{B}_4$  type boride phase; (b) microstructure  
 222 after etching; Nd-rich phases are etched away and nanocrystalline  $\text{Nd}_2\text{Fe}_{14}\text{B}$  matrix grains are microscopically exposed; an inset  
 223 shows  $\text{Nd}_2\text{O}_3$  oxide phase marked with "3"; (c) higher magnification image of matrix phase consisting of mostly nanosized grains  
 224 and approx. < 5 vol. % fraction of large  $\text{Nd}_2\text{Fe}_{14}\text{B}$  "R"- residual grains (not reacted during the HDDR process); (d) 50,000X  
 225 magnification of a powder particle fracture surface showing 240 – 420 nm single crystal  $\text{Nd}_2\text{Fe}_{14}\text{B}$  grains.  
 226

Table 1: EDS quantification of different phases in the recycled HDDR powder.

Phase Number	Phases	Nd (at. %)	Fe (at. %)	B (at. %)	O (at. %)	Nb (at. %)	Al (at. %)
1	$\text{Nd}_2\text{Fe}_{14}\text{B}$ Matrix	12.7	87.1	-	-	-	1.2
2	Nd-rich $\text{NdO}_x/\text{NdO}_2$	24.6	29.5	-	46.3	-	-
3	$\text{Nd}_2\text{O}_3$	35.2	12.2	-	47.3	-	-
4	$\text{NbFe}_2$ Laves	0.7	47.6	-	-	51.7	-
5	$\text{NdFe}_4\text{B}_4$ Boride	10.9	39.6	-	2.5	-	-

227  
 \* Corresponding Author.  
 Email: [awais.ikram@ijs.si](mailto:awais.ikram@ijs.si) (Awais Ikram)

228 Upon etching the matrix grains became more apparent and are shown in Figure 3 (b), as the Nd-rich phases were  
229 selectively removed, except the  $\text{Nd}_2\text{O}_3$  oxides (as the bright phase marked as 3 in the inset of Fig. 3b). Most of the  
230 bright phases along the grain boundaries have an approximate atomic ratio Nd:O of 1:2 (Table 1) which indicates the  
231 chemical composition to  $\text{NdO}_x$  ( $\text{NdO}_2$ ) type Nd-rich phases. The protruding light greyish Nd-rich features with Nd:O  
232 elemental ratio of 2:3 (Table 1), pointing to the presence of  $\text{Nd}_2\text{O}_3$  type oxide as identified with the XRD. These  
233 oxides are randomly scattered in the recycled HDDR powder along the particle boundaries as obvious after etching in  
234 Figure 3 (b), appearing in different morphologies and composition as discussed. The traces of Al were also observed  
235 at the interfaces of the Nd-rich grain boundaries and the  $\text{Nd}_2\text{Fe}_{14}\text{B}$  matrix grains. The Al signal was also detected  
236 within the  $\text{Nd}_2\text{Fe}_{14}\text{B}$  grains, and measured EDS values correspond to an overall  $\leq 1.2$  at. % Al in the Nd-Fe-B matrix  
237 phase. The Al addition has been reported to decrease the melting point of rare earth rich (Nd, Dy) grain boundary  
238 phase [32]. K. Morimoto et al. (2012) [33] reported that the addition of up to 2.5 at. % of Al causes the thickening of  
239 the Nd-rich grain boundary phase. Al is known to uniformly distribute the Nd-enriched phase from the triple  
240 junctions along the grain boundaries. This pins the domain walls at the grain boundaries and improves the isolation  
241 of the adjacent  $\text{Nd}_2\text{Fe}_{14}\text{B}$  grains, increasing the overall powder  $H_{ci}$  [33 - 35]. Higher magnification image of the  
242 nanocrystalline matrix grains in the recycled HDDR powder after etching is shown in Figure 3 (c) and (d), with an  
243 average grain size in the range from 240 – 420 nm and a monomodal grain size distribution. In addition, there are  
244 also larger “residual” (marked as “R”) micron-sized grains (2 – 10  $\mu\text{m}$ ) observed within the initial recycled powder  
245 which can be attributed to the incomplete HDDR reaction [29, 52].  
246

### 247 **3.3 Magnetic Properties and characterization of SPS reprocessed HDDR powder.**

248 After the HDDR reprocessing, the coercivity of the recycled powder as measured with the VSM (without self-  
249 demagnetization adjustment) was 830 kA/m. The first objective of our study was to find a range of SPS processing  
250 temperature where the recycled HDDR powder could be densified completely. The magnetic properties and density  
251 measurements for SPS-ed magnets in range of 650 – 850  $^{\circ}\text{C}$  and holding time of 1 minute as shown in Figure 4  
252 indicate a very good possibility of obtaining fully dense Nd-Fe-B permanent magnets from recycled HDDR powders  
253 with SPS. At 650  $^{\circ}\text{C}$ , the magnet density was only 91% of the theoretical value, however, the density was found to  
254 increase monotonically with the temperature and at  $T \geq 700$   $^{\circ}\text{C}$  where it starts to approach the theoretical value of  
255 7.58  $\text{g}/\text{cm}^3$ . Here we have to emphasize that it is possible to sinter the scrap Nd-Fe-B with the oxygen content  
256 greater than 4500 ppm even though it is known that Nd-oxide phases don't sinter well [44 - 47].

\* Corresponding Author.

Email: [awais.ikram@ijs.si](mailto:awais.ikram@ijs.si) (Awais Ikram)

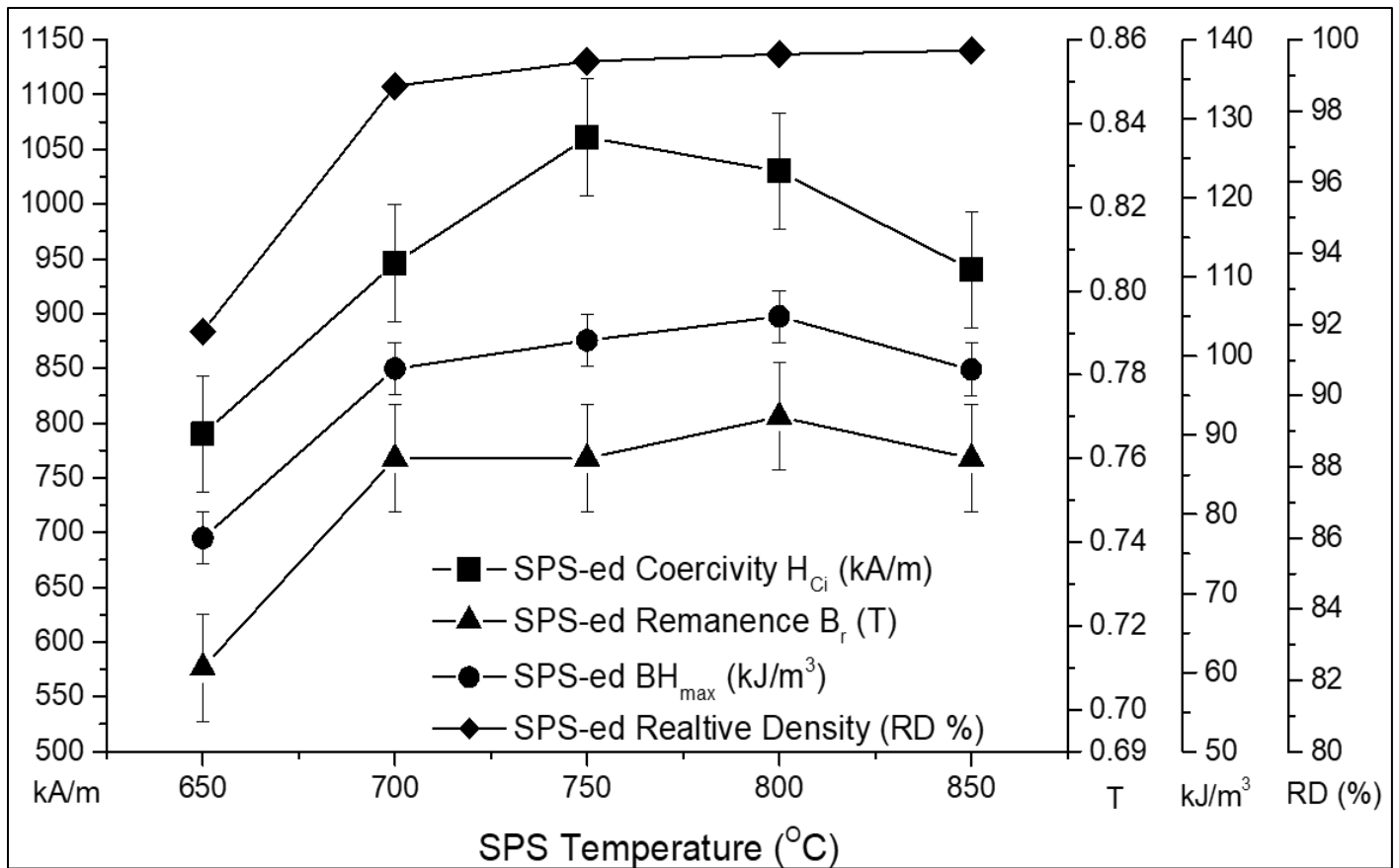


Figure 4: the effect of SPS temperature on  $H_{Ci}$ ,  $B_r$ ,  $BH_{max}$  and density of the recycled HDDR Nd-Fe-B powders.

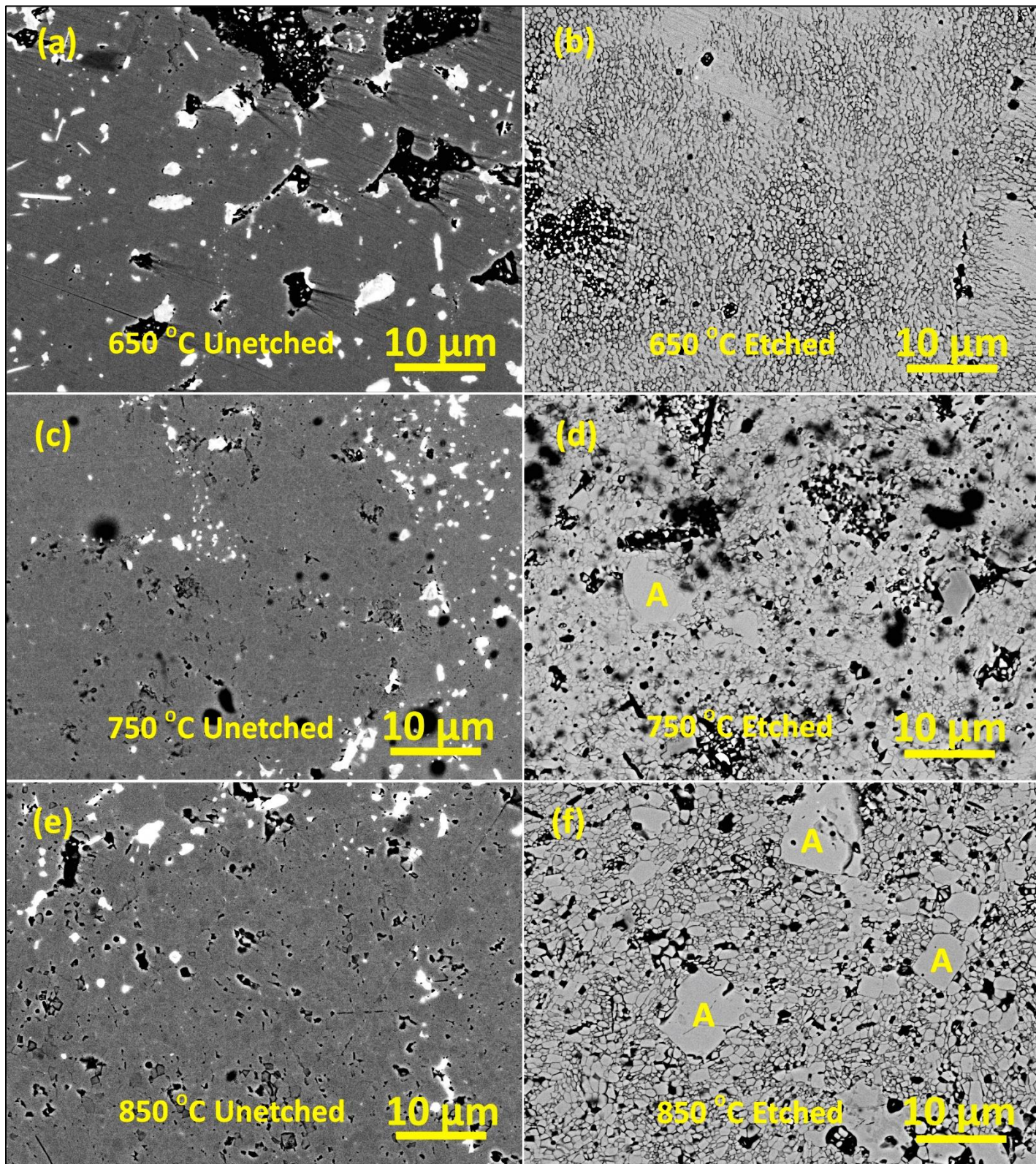
Figure 4. shows that nearly full densification is possible due to grain consolidation and effective pore elimination with the SPS. The  $BH_{max}$  increases simultaneously with the  $B_r$ , which was found to increase with the reprocessing temperatures above 700 °C and reached the value of 0.77 T (105 kJ/m<sup>3</sup>) in the sample SPS-ed at 800 °C. Since the powder particles are not aligned before the SPS, the measured remanence in this range (0.71 – 0.77 T) implies the isotropic nature of the Nd-Fe-B reprocessed magnets.

The recycled powder  $H_{Ci}$  = 830 kA/m increased further with SPS reprocessing temperature of 700 °C and reached a maximum value of 1061 ± 50 kA/m at the optimal SPS temperature of 750 °C as shown in Figure 4. With the further increase in temperature, the  $H_{Ci}$  drops down slightly which can be associated with moderate grain growth. With increased oxygen content in the scrap magnet from 2660 ppm to 4760 ppm after HDDR reprocessing, one would expect slower sintering kinetics of the recycled HDDR powder, as some of the metallic Nd is scavenged by oxygen. So with a reduction of the overall Nd content i.e. the Nd-rich liquid phase, proper wetting of the grain boundary phase will be limited. The Nd oxides ( $Nd_2O_3$  and  $NdO_2$ ) remain in the solid state during sintering and appear along the triple pockets and the grain junctions. In the HDDR system, the matrix grains and grain boundary phases are nanosized, with a significantly higher surface area, so the regions for Nd scavenging and oxide precipitation are considerably higher. In order to increase the  $H_{Ci}$  of sintered [32] and the HDDR powder [33 – 34], the rare earth rich low-temperature eutectic alloys are blended into the compositions with leaner rare-earth content, which provides enough intergranular paramagnetic Nd-rich phase for the intergrain decoupling [24 – 26]. In the conventional

\* Corresponding Author.

Email: [awais.ikram@ijs.si](mailto:awais.ikram@ijs.si) (Awais Ikram)

278 vacuum sintering route, the oxygen content is always kept below the 4000 ppm limit for sinterability and usually, the  
279 excess amount of  $\text{NdH}_2$  is added to counter the Nd-enrichment loss due to oxidation [10, 15]. On the contrary, SPS  
280 enables concurrent localized coalescence/melting [48 – 50] of the Nd-rich grain boundary phase in the bulk powder,  
281 which promotes the wetting of the particles even with  $\text{O}_2 \sim 5000$  ppm, therefore to an experimentally identified limit  
282 of  $\text{O}_2 < 8000$  ppm, sintering of the HDDR reprocessed scrap is possible with the SPS.  
283



284

285 *Figure 5: BSE SEM micrographs of SPS-ed specimen: unetched surface at (a) 650 °C (c) 750 °C and (e) 850 °C; and etched surfaces*  
286 *showing grain structure at (b) 650 °C (d) 750 °C and (f) 850 °C. The increment of SPS temperatures from 650 – 850 °C indicates*  
287 *the evident grain coarsening at higher reprocessing temperatures; “A” features abnormal grain coarsening in samples SPS-ed at*  
288 *elevated temperatures.*

289  
290 The SPS experiments performed at 650 °C were below the eutectic temperature of the ternary phase transition ( $\alpha$ -  
291 Nd + Nd<sub>2</sub>Fe<sub>14</sub>B and NdFe<sub>4</sub>B<sub>4</sub>). In this case, we can only expect solid-state mass transport and Nd-rich phase will not  
292 experience redistribution, although rearrangement of the particles is made under 50 MPa uniaxial pressure. So the  
293 SPS coalescence together these particles with high heat transfer at particle necking regions by pulsed current  
294 resistance heating [48] and in effect the short range mass transport only fills out few pores which are apparent from  
295 the density of 6.9 g/cm<sup>3</sup> (91% densification). Figure 5 (a) shows the unetched surface of sample SPS-ed at 650 °C,  
296 which can be correlated similarly to the recycled HDDR powder in terms of phase distribution and with several pores  
297 present, density is apparently lower (~90% densification). After etching in Figure 5 (b), the average grain size range  
298 of SPS-ed samples at 650 °C is between 280 - 440 nm, with an exception of few larger sized grains approx. 1  $\mu$ m. The  
299 SPS process changes from solid state sintering to liquid phase sintering when the SPS holding temperature is raised  
300 to 700 °C, which is above the ternary eutectic temperature. Under pressure, the recycled powder particles rearrange  
301 and the liquid phase diffuses towards the center of the powder particles into the grain boundaries at  $T \geq 700$  °C. A  
302 slightly higher temperature of 750 °C is optimal for the grain boundary diffusion during SPS, such that mass transport  
303 is efficient enough for near complete densification (99 %) and pore annihilation as observed in the unetched  
304 specimen in Figure 5 (c), but retaining a control with minimal grain growth as observed after etching in Figure 5 (d).  
305 Near the Nd-rich pools the grain boundary phase acts as the spacers phase between the matrix grains, but the  
306 overall distribution of the grain boundary phase along the matrix grains and the particles are not uniform. The grain  
307 size distribution of recycled HDDR powder SPS-ed at 750 °C corresponds to  $330 \pm 120$  nm. Apart from normally  
308 grown nanocrystalline grains of  $330 \pm 120$  nm size at 750 °C, the slightly larger residual grains ( $\geq 5$   $\mu$ m) were also  
309 observed. When the SPS holding temperature was 850 °C, the coarsening of these “nanocrystalline” grains becomes  
310 apparent with an increase in average grain size to  $750 \pm 260$  nm and some grains larger than several microns were  
311 also observed. At  $T_{SPS} > 850$  °C, the grain growth rate is faster than the pore mobility which leads to the isolation of  
312 the pores within larger grains as neighboring grains coalesce together rapidly and begin to merge with a higher  
313 degree of faceting [51]. This results in the abnormal grain growth labelled with “A” in Figure 5 (d and f), that causes  
314 the bimodal grain size distribution. This abnormal grain growth in samples SPS-ed at  $T > 800$  °C is also one of the  
315 reasons for the  $H_{Ci}$  reduction.

316  
317 The redistribution of the Nd-rich phase between the matrix grains is considered to improve the localized decoupling  
318 effect which increases the  $H_{Ci}$  [24, 33-35]. Immediately after the removal of heat, the reprecipitation [51] of 2:14:1  
319 matrix grains from solidifying Nd-rich phase causes pore eradication as the diffusion in the liquid phase augments  
320 the surfaces of the nanocrystalline grains and the grain boundary interfaces such that full densification is possible.  
321 This quick non-equilibrium sintering prevents any excessive mass transport of the liquid phase, and as the current

\* Corresponding Author.

Email: [awais.ikram@ijs.si](mailto:awais.ikram@ijs.si) (Awais Ikram)

322 stops, the cooling begins immediately which prevents grain coarsening [38]. Due to the lack of Nd-rich phase at the  
323 grain boundaries in the commercial grade, HDDR powders after SPS-ing is accounted for a drastic  $H_{Ci}$  drop since the  
324 Nd-rich phase is absent between matrix grains and a significant localized exchange coupling effect may be predicted  
325 [24]. In the recycled HDDR powders, the Nd-rich phase was available at the particle boundaries of EOL magnets after  
326 the completion of d-HDDR reaction which then experienced the redistribution via liquidus state transformation  
327 during the SPS reprocessing at  $T \geq 700$  °C. Therefore, the  $H_{Ci}$  of SPS-ed magnets is higher than the starting recycled  
328 HDDR powder. It is evident that SPS allows controlled high heating rates which are suitable for rapid sintering of  
329 dense materials. The pulsed current and resistance heating at interparticle interfaces create very high localized  
330 temperature profiles, such that extensive mass transport is enhanced by grain boundary diffusion and pore  
331 annihilation [48, 50]. Subsequently, faster cooling rates prevent the long-range diffusional transformation and grain  
332 growth can be controlled.

### 334 **3.4 Magnetic properties and characterization of SPS-ed and thermally treated recycled HDDR powder**

335 The effect of thermal treatment annealing was further studied on the recycled HDDR powder treated with SPS. The  
336 750 °C temperature for 15 minutes holding time was chosen to compare the findings with the previous findings of K.  
337 Takagi et al [23]. Thermal treatment temperature ternary eutectic point of 665 °C is set such that equilibrium  
338 diffusional mass transport can take place [51], and the Nd-rich phase can penetrate more intergranular channels so  
339 that the grain boundary phase distribution becomes more uniform. This temperature has experimentally proven to  
340 prevent the grain coarsening, which will certainly reduce the  $H_{Ci}$ . This post SPS annealing temperature cannot be  
341 reciprocated within the SPS furnace due to a different localized heating mechanism [48 - 50]. In SPS, the excessive  
342 localized heating at interparticle contacts will contribute to the coarsening of the Nd-rich pools as well as the  
343 nanocrystalline grains. Since the Nd-rich phase will not be uniformly distributed as required for improving the  $H_{Ci}$ ,  
344 further prolonging the holding time at 750 °C in the SPS has degraded the magnetic properties as shown in Table 2  
345 (see below). Under conventional annealing treatments, the equilibrium diffusional heating [51] is applicable and the  
346 Nd-rich phase is allowed to redistribute via concentration gradients along the matrix grain surfaces [45 – 47].

\* Corresponding Author.

Email: [awais.ikram@ijs.si](mailto:awais.ikram@ijs.si) (Awais Ikram)

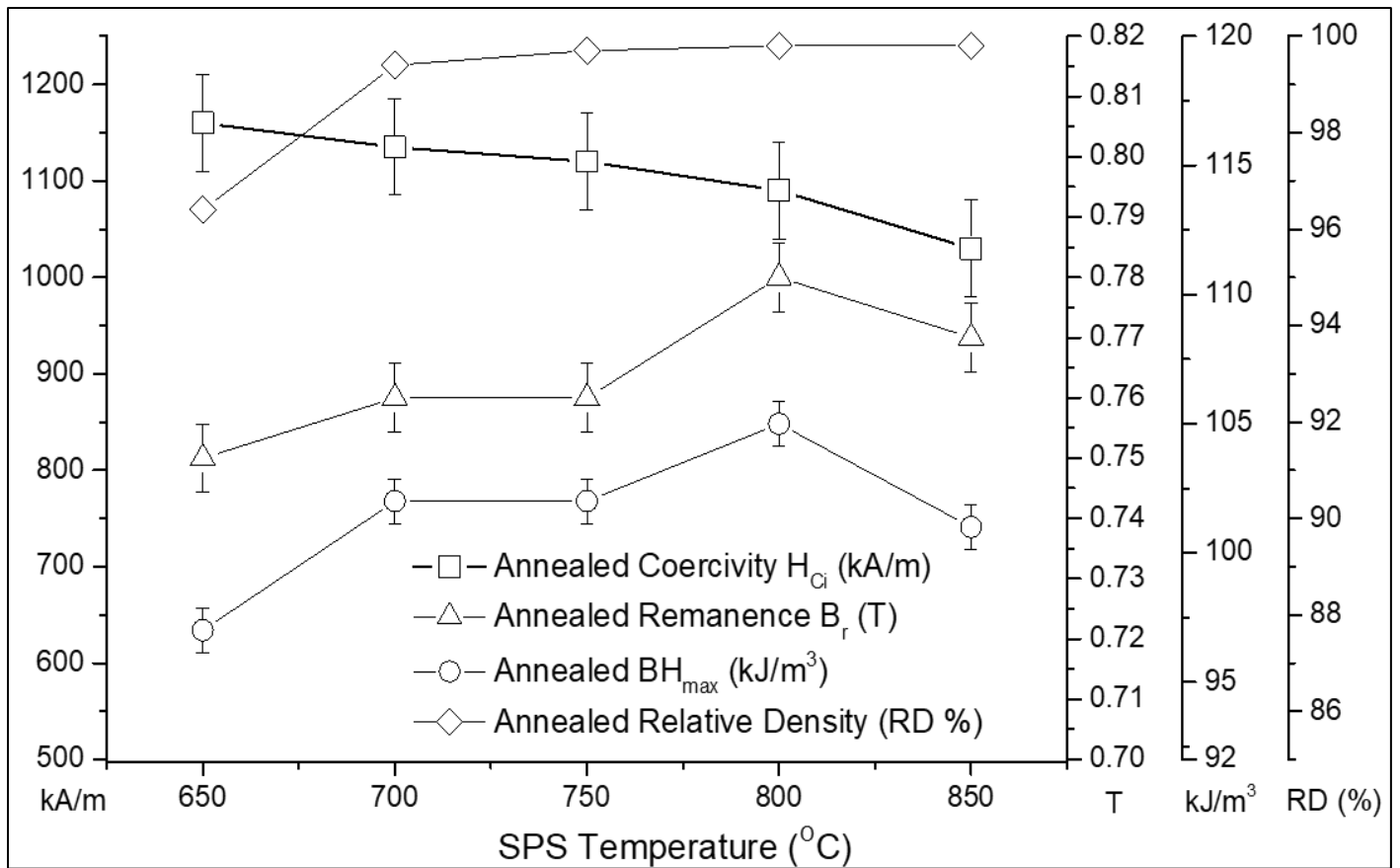


Figure 6: the effect of post-SPS thermal treatment at 750 °C for 15 minutes on the  $H_{Ci}$ ,  $B_r$ ,  $BH_{max}$  and densification of the reprocessed HDDR Nd-Fe-B powders.

The trend in Figure 6 shows a comparative increase in  $H_{Ci}$  of thermally treated samples over that of the as SPS-ed samples (Fig. 4), but the  $H_{Ci}$  increase is milder in samples SPS-ed at temperatures higher than 750 °C. The sample SPS-ed at 650 °C experienced a substantial improvement in the  $H_{Ci}$  = 1160 kA/m from 790 kA/m. This is approximately 30 % higher than the starting HDDR powder. The  $H_{Ci}$  increased only slightly for thermally treated samples SPS-ed at 850 °C due to the breach of grain growth temperature above 820 °C [23]. The  $B_r$ ,  $BH_{max}$  and density of the thermally treated samples also experienced a mild improvement in absolute values in all cases as shown in Figure 6. After the thermal treatment  $B_r$  = 0.78 T and  $BH_{max}$  = 105 kJ/m<sup>3</sup> was measured for the sample SPS-ed at 800 °C; however, the  $J_r/J_s$  ratio of 0.54 reaffirmed the ‘isotropic nature’ of reprocessed magnets. In the sample SPS-ed 850 °C a notable reduction in  $H_{Ci}$  negates the application of higher SPS temperatures for the recycled HDDR powder since this temperature is above the grain growth temperature [23].

The post-SPS equilibrium diffusion controlled thermal treatment is done to uniformly redistribute this liquid Nd-rich phase, smoothen the matrix and grain boundary interface, by reducing the interfacial strains associated with hcp Nd<sub>2</sub>O<sub>3</sub> formation [23, 25, 35, 40]. Therefore these treatments have also been reported to increase the  $H_{Ci}$  by the redistribution of Nd-rich grain boundary phase surrounding Nd<sub>2</sub>Fe<sub>14</sub>B grains in sintered magnets [40 - 42] due to the localized decoupling of Nd<sub>2</sub>Fe<sub>14</sub>B grains. Similarly, in the HDDR Nd-Fe-B magnets, the effect of localized decoupling can be combined with the domain wall pinning effect of the grain boundaries [23, 35]. For the HDDR powders, the post-sinter annealing mechanism for the  $H_{Ci}$  improvement to date is not fully understood. According to K. Takagi et

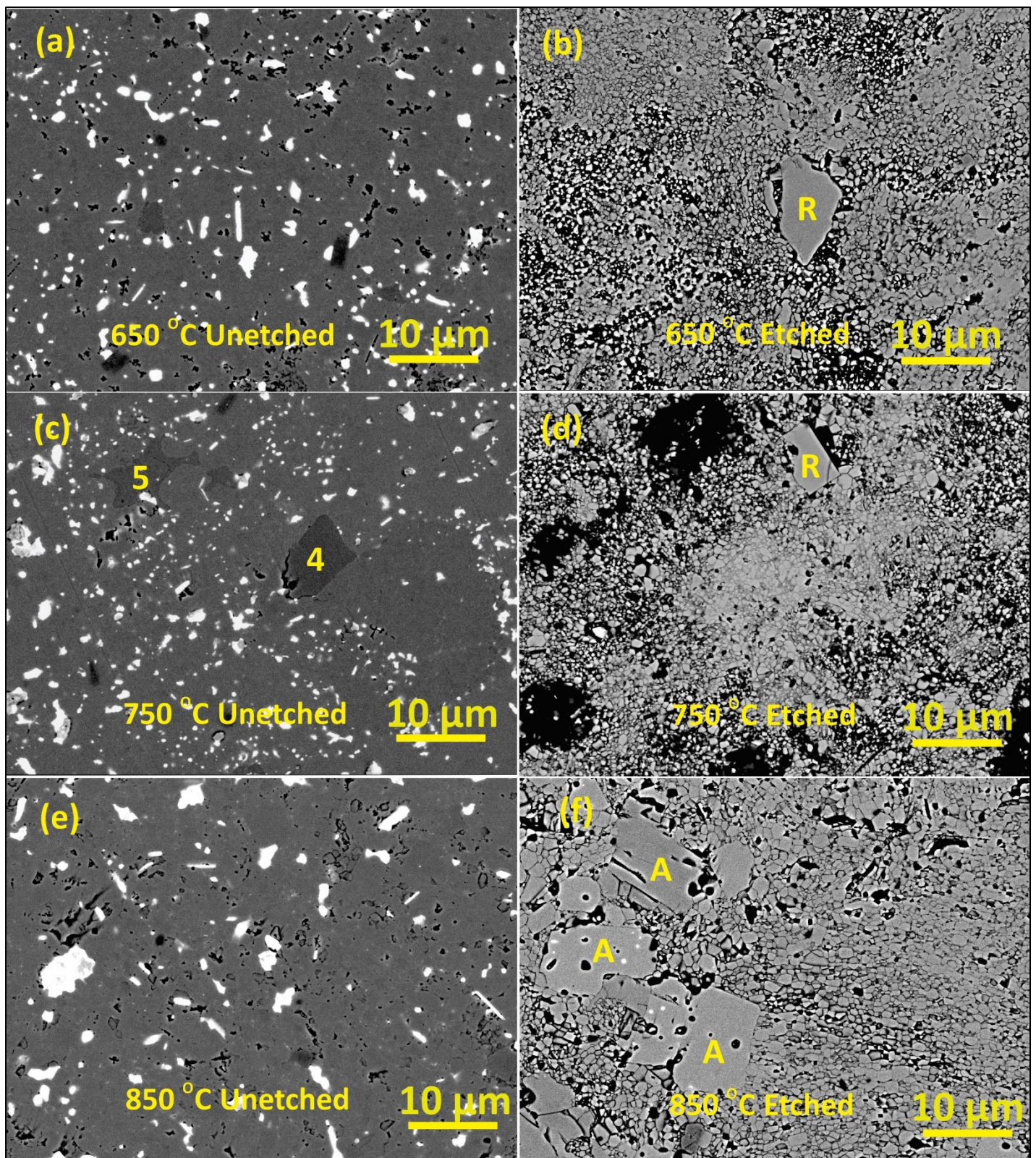
\* Corresponding Author.

Email: [awais.ikram@ijs.si](mailto:awais.ikram@ijs.si) (Awais Ikram)

369 al. [23] the relaxation of interfacial strains is believed to improve the  $H_{Ci}$  in SPS-ed HDDR type magnets and  
370 suggested annealing did not change the thickness of the grain boundary phase. Whereby Li et al. [40], proposed the  
371 increase in  $H_{Ci}$  after annealing is due to the widening of the amorphous Nd-rich grain boundary phase. According to  
372 W. Mo et al. [46], the grain boundary phase transforms from crystalline to amorphous as its thicknesses decrease,  
373 and in the case of HDDR Nd-Fe-B the grain boundary thickness varies from 1.6 – 3.0 nm only [23, 33 – 35]. The  
374 thermal treatment temperature of 750 °C is adequately higher than the ternary eutectic ( $T_{ELM}$ ) = 665 °C, so according  
375 to the pseudobinary phase diagram [39], the  $Nd_2Fe_{14}B$  matrix and  $NdFe_4B_4$  phases are in solid state but only the Nd-  
376 rich phase melts and undergoes diffusion controlled redistribution and therefore the thermal treatment should not  
377 contribute to grain growth significantly. The Nd oxide phases (hcp  $Nd_2O_3$  and fcc  $NdO_x$ ) also remain in the solid state  
378 during SPS-ing and thermal treatment but can experience the relaxation of the localized strain fields. Since  $T_{ELM}$  gets  
379 reduced due to the presence of Dy and Al from 685 °C to 665 °C [39], the Nd-rich phase must have high mobility at  
380 750 °C for grain boundary diffusion, developing a controlled Nd-rich/ $Nd_2Fe_{14}B$  interfacial microstructure for higher  
381  $H_{Ci}$ . Therefore, one may speculate the redistribution of Nd-rich phase and relaxation of interfacial strains (at  
382  $Nd_2Fe_{14}B$  matrix grains, Nd-rich grain boundary phase and Nd oxide interjunctions) as a combined mechanism behind  
383 the  $H_{Ci}$  improvement in the SPS-ed and post-annealed HDDR system. When the SPS temperature is higher than  $T_{ELM}$ ,  
384 then the short-range redistribution of the grain boundary phase can be attributed to the increased  $H_{Ci}$ . The complex  
385 microstructural effects associated with the Nd-rich phase and the interfacial grain chemistry as the governing  
386 mechanism behind the  $H_{Ci}$  enhancement in the HDDR powder is not properly understood. The  $H_{Ci}$  increase in the  
387 HDDR powder is associated with increased grain boundary width for effective grain decoupling from the  
388 ferromagnetic intergranular phase [33 – 35] as well as strain relaxation effects after the thermal treatment [23].

\* Corresponding Author.

Email: [awais.ikram@ijs.si](mailto:awais.ikram@ijs.si) (Awais Ikram)



389  
 390 *Figure 7: BSE SEM micrographs of post SPS thermally treated: non-etched samples with better redistribution of Nd-rich grain*  
 391 *boundary phase at (a) 650 °C (c) 750 °C and (e) 850 °C; and grain morphology of etched SPS-ed specimen at (b) 650 °C (d) 750 °C*  
 392 *and (f) 850 °C; the grain marked with "R" indicate untransformed residual grains from EOL scrap magnet, "A" abnormally grown*  
 393 *grains, "L" is NbFe<sub>2</sub> Type-Laves phase and "B" indicates tetragonal NdFe<sub>4</sub>B<sub>4</sub> phase.*  
 394

395 The most prominent feature from the microstructural comparison of SPS-ed unetched samples in Figure 5 (a, c and  
 396 e) with the post SPS thermally treated samples in Figure 7 (a, c and e) attributed to the redistribution of the Nd-rich

\* Corresponding Author.

Email: [awais.ikram@ijs.si](mailto:awais.ikram@ijs.si) (Awais Ikram)

397 phase such that the areal fraction of thermally treated samples is higher than SPS reprocessed samples. On the  
398 contrary, when thermally treated specimens were etched, the difference in average grain size was minimal after the  
399 thermal treatment as evident in Figure 7 (b, d and f) for 650, 750 and 850 °C respectively for the SPS reprocessed  
400 samples. Apart from normally grown nanocrystalline grains, the residual grains “R” from the EOL scrap magnets were  
401 also observed in the etched samples as shown in Figure 7 (b and d). When the SPS reprocessing temperature was  
402 650 °C, these residual grains were present without any expected increase in size because of the unavailability of the  
403 liquid phase to allow diffusion and grain growth [51]. The residual grains start faceting at  $T > 750$  °C such that these  
404 large sized residual grains with more than 6 facets allow size augmentation due to excess thermal energy available at  
405 elevated SPS temperatures and so the normal grain growth is commenced [33]. At SPS temperature set at 850 °C,  
406 the residual, as well as larger nanocrystalline matrix grains, start consuming smaller grains and now the mechanism  
407 of grain growth proceeds to abnormal grain coarsening as shown in Figure 7 (f). The abnormally coarsened grains  
408 contain isolated porosity, which makes them easier to distinguish from the residual grains. When the grain growth  
409 rate is higher than the pore mobility and the pores have surface energy higher than the grain boundary energy, then  
410 these pores get isolated within the abnormally coarsened grains and do not annihilate [51]. This, in turn, degrades  
411 the  $H_{ci}$  at complete densification, as shown for thermally treated samples in Figure 6.

412  
413 From figure 8 (a) it can be observed that the 2:14:1 matrix grains are surrounded by the Nd-rich phase in the region  
414 approximately 1 – 2  $\mu\text{m}$  away from the spot where Nd-rich phase has solidified after the SPS. The  $\text{Nd}_2\text{Fe}_{14}\text{B}$  grains,  
415 further away approx. 10 – 20  $\mu\text{m}$  from this region with the solidified Nd-rich phase, are observed to be in intimate  
416 contact with each other, as the grain boundary Nd-rich phase is absent or inadequately redistributed due to most  
417 probably short sintering times (10 minutes in total) and low temperatures ( $< 750$  °C) used in SPS.

418  
419 After the thermal treatment performed in vacuum at 750 °C for 15 minutes, where the diffusion of the liquid phase  
420 is favorable (as the temperature exceeds the melting point of the Nd-rich phase), therefore the Nd-rich phase better  
421 surrounds the  $\text{Nd}_2\text{Fe}_{14}\text{B}$  grains than in the SPS-ed samples from the condensed liquid phase. In the post thermally  
422 treated sample presented in Figure 8 (b) it can be observed that instead of the Nd-pool a cavity appears in its place  
423 indicating to the Nd-rich phase has redistributed along the grain boundary channels to higher extent and longer  
424 lengths than in the SPS-ed only sample, as in figure 8 (a). This, in turn, results in an improvement in  $H_{ci}$ , which was  
425 only slight for temperatures above 750 °C. This indicates that the SPS reprocessing parameters, especially the  
426 current density and temperature, have a more significant effect in developing the final microstructure and the  
427 magnetic properties. The thermal treatments are considered as a complementary process to further augment the  
428 magnetic properties by relieving the microstructure of the stresses and redistribution of RE-rich grain boundary  
429 phase [23, 25, 35, 40].

430  
\* Corresponding Author.

Email: [awais.ikram@ijs.si](mailto:awais.ikram@ijs.si) (Awais Ikram)

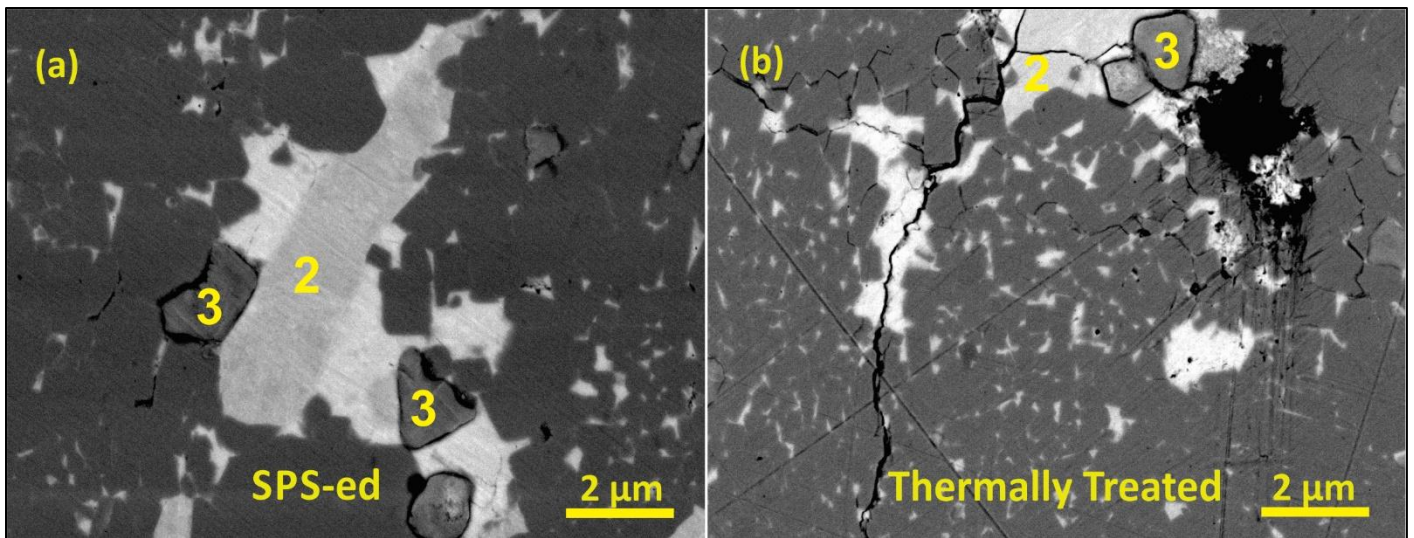


Figure 8: high magnification micrographs showing the effect of grain boundary phase redistribution in (a) as SPS-ed sample synthesized at 750 °C and (b) thermally treated after SPS Phase 2 and 3 corresponds to Nd-rich phase and Nd<sub>2</sub>O<sub>3</sub> respectively.

The study also examined how the magnetic properties of the reprocessed HDDR powder are influenced by the alteration of two SPS processing conditions: the holding time (1 and/or 5 minutes) and the SPS heating rate (50 and/or 100 °C/min), as shown in Table 2. The arrows (↓) in table 2 indicate the improvement in the magnetic properties of SPS-ed magnets after the thermal treatment at 750 °C for 15 minutes. This helped in determining the optimal reprocessing conditions at 50 MPa applied uniaxial pressure. The observed trend of best achieved magnetic properties (green table), as shown in Figure 4 and 6, was by keeping the heating rate of 100 °C/minute and short holding time of 1 minute only. Slowing the thermal ramp to 50 °C/minute did not add any improvement to the former case, so a rapid reprocessing approach is not detrimental as long as current density in the SPS is kept optimal [48, 50]. Slower ramps slacken the short-range diffusivity and the redistribution of the Nd-rich liquid phase diminishes due to a lower SPS current density. At SPS temperature of 750 °C, the drop in H<sub>ci</sub> is insignificant even by prolonging the holding time due to better diffusion kinetics of the Nd-rich liquid phase. The magnetic properties degraded severely when the SPS temperature was higher than 820 °C, which is associated with the abnormal grain growth [23, 37] and the results (from Figure 5 and 7 of samples SPS-ed at 850 °C) are in agreement with these findings. Therefore, reducing the ramp at higher temperatures permits excess thermal energy to the system for grain coarsening. In the last case, when the holding temperature was increased to 5 minutes and the ramp was optimized to 100 °C/minute, the only persistent improvement observed was in the densification of the SPS-ed and thermally treated samples. The H<sub>ci</sub> was consistently higher than slower ramped samples (50 °C/min), but nonetheless, H<sub>ci</sub> was slightly lower than for the shorter holding time of 1 minute. Although it can be expected that with higher overall densification, B<sub>r</sub>, in turn, should increase, but the maximum value 0.75 T achieved disapproves the prolonged SPS holding times. Moreover, the abnormal grain growth kinetics can be activated with longer holding time and higher temperatures [48]. So by purpose, the SPS process has been verified as a significantly advantageous tool if the appropriate parameters are set for rapid sintering operations.

\* Corresponding Author.

Email: [awais.ikram@ijs.si](mailto:awais.ikram@ijs.si) (Awais Ikram)

**Table 2: The variation of magnetic properties by altering SPS conditions and the improvement with annealing.**

SPS Conditions ↓	100 °C/min Ramp and 1 minute holding time.			50 °C/min Ramp and 1 minute holding time.			100 °C/min Ramp and 5 minute holding time.		
SPS Temperature (°C)	H <sub>ci</sub> (kA/m)	B <sub>r</sub> (T)	Density (g/cm <sup>3</sup> )	H <sub>ci</sub> (kA/m)	B <sub>r</sub> (T)	Density (g/cm <sup>3</sup> )	H <sub>ci</sub> (kA/m)	B <sub>r</sub> (T)	Density (g/cm <sup>3</sup> )
650	790	0.71	6.96	741	0.69	7.01	781	0.68	7.13
	↓	↓	↓	↓	↓	↓	↓	↓	↓
700	1160	0.75	7.31	1130	0.72	7.08	1140	0.70	7.42
	↓	↓	↓	↓	↓	↓	↓	↓	↓
750	946	0.76	7.49	893	0.74	7.36	888	0.74	7.51
	↓	↓	↓	↓	↓	↓	↓	↓	↓
800	1135	0.76	7.54	1108	0.75	7.39	1107	0.75	7.56
	↓	↓	↓	↓	↓	↓	↓	↓	↓
850	1061	0.76	7.54	1019	0.76	7.53	1040	0.75	7.56
	↓	↓	↓	↓	↓	↓	↓	↓	↓
850	1120	0.77	7.56	1100	0.77	7.55	1102	0.75	7.57
	↓	↓	↓	↓	↓	↓	↓	↓	↓
850	1030	0.77	7.55	980	0.76	7.55	992	0.75	7.57
	↓	↓	↓	↓	↓	↓	↓	↓	↓
850	1090	0.78	7.57	1074	0.77	7.56	1064	0.75	7.58
	↓	↓	↓	↓	↓	↓	↓	↓	↓
850	940	0.76	7.56	700	0.68	7.53	855	0.72	7.57
	↓	↓	↓	↓	↓	↓	↓	↓	↓
850	1030	0.77	7.57	790	0.69	7.56	953	0.74	7.58
	↓	↓	↓	↓	↓	↓	↓	↓	↓

459

460

461

462

463

464

465

466

467

468

469

470

471

472

It is imperative to mention that SPS reprocessing is one of the few suitable techniques to obtain fully dense and high coercivity sintered magnets from the recycled HDDR powder since conventional vacuum sintering was not applicable to the recycled scrap and to our experience have produced poor results. This lack of sinterability in conventional vacuum sintering of the recycled HDDR powder is associated with the poor grain boundary phase mobility and redistribution even at 1050 °C, therefore the powder particles do not coalesce together even in a well prepared green compact up to 100 MPa pressure. The simultaneous application of pressure and localized heating of powder particles in SPS allows the sintering to develop bulk magnet from scrap magnetic powders.

To summarize, the recycled HDDR Nd-Fe-B powder was subjected to a thorough SPS treatment. In all conditions, the coercivities of sintered magnets were higher than the starting recycled HDDR powder of average size 240 ± 100 nm due to the grain size preservation after the SPS reprocessing. The optimal temperature range of 750 - 800 °C for developing SPS-ed magnets was identified for reaching nearly full density and H<sub>ci</sub> higher than the starting recycled HDDR powder. Post SPS thermal treatment at 750 °C for 15 minutes increased the H<sub>ci</sub> due to the redistribution of

\* Corresponding Author.

Email: [awais.ikram@ijs.si](mailto:awais.ikram@ijs.si) (Awais Ikram)

473 thin Nd-rich grain boundary phase between the matrix grains, as confirmed by HR-SEM. The effect of redistribution is  
474 pronounced after thermal treatment above eutectic temperature on the samples SPS-ed at 650 °C due to limited  
475 diffusion in the solid state SPS. Whereby above the eutectic point, the sample SPS-ed at 700 °C experienced a higher  
476 degree of wetting of the matrix grains and subsequently the  $H_{Ci}$  was high after SPS. The SPS-ed samples reached peak  
477  $H_{Ci}$  of 1060 kA/m value after SPS at 750 °C, whereby the full densification was achieved by SPS at 800 °C which can  
478 be associated with effective pore elimination. The post-SPS thermal treatment resulted in the  $H_{Ci}$  improvement up to  
479 30% higher than the starting recycled HDDR powder. The samples SPS-ed at lower temperatures like 650 – 750 °C  
480 experienced improvement in the  $H_{Ci}$  due to better redistribution of Nd-enrichments from the particle to the grain  
481 boundaries. No evidence of abnormal grain growth was observed after the subsequent reprocessing with SPS and  
482 thermal treatment under the optimum conditions. The average grain size of samples SPS-ed at 650 °C and 750 °C  
483 were  $280 \pm 120$  nm, and  $330 \pm 120$  nm respectively. Post thermal treatments did not exaggerate the grain size and  
484 the average grain size only experienced a modest increment of approx. 100 – 200 nm. The magnetic properties begin  
485 to deteriorate when SPS temperature was greater than 800 °C due to a breach of grain growth temperature and  
486 defect generation due to localized overheating during the SPS. While the samples SPS-ed at  $T \geq 850$  °C, a modest  
487 gain in the  $H_{Ci}$  was reported after the thermal treatment, which may be associated only with the relaxation of the  
488 interfacial strains introduced by defects generation along the coarser grains. For the samples SPS-ed at 850 °C the  
489 normal grains ranged from  $400 \pm 250$  nm whereby coarser grains extended from 750 – 2600 nm making a bimodal  
490 size distribution. Slowing down the SPS heating rate to 50 °C/minute did not add to the improvement of the  $H_{Ci}$ .  
491 Also, increasing the holding time to 5 minutes only improved the densification, but not the  $H_{Ci}$ . Disclosing the  
492 mechanism behind  $H_{Ci}$  enhancement in terms of the microstructure after SPS reprocessing and the post-sinter  
493 thermal treatment signifies the magnetic performance relationship to develop suitable reuse and recyclability of the  
494 EOL/scrap magnets as well as the applicability of SPS reprocessed permanent magnets.

## 495 4. Conclusions

496 The two accomplished goals of this study include: reprocessing of the recycled HDDR Nd-Fe-B powders with SPS and  
497 thermal treatment in combination delivered fully dense bulk magnets with  $H_{Ci}$  values synonymous to the SPS-ed  
498 commercial grade Aichi Steel's HDDR powder. Secondly, even with a high oxygen content in the recycled powders (~  
499 4760 ppm), sinterability was not lost and the SPS-ed  $H_{Ci}$  was higher than the starting HDDR. This route also verified  
500 100% preservation of  $H_{Ci}$  of the EOL scrap magnets by HDDR nano structurization and subsequent SPS treatment.  
501 The SPS performed below the eutectic do not provide enough grain boundary phase in the liquid state, so after the  
502 thermal treatment at 750 °C, which is above the eutectic temperature, the melt formation wets the grain boundaries  
503 and  $H_{Ci}$  is increased due to a better redistribution of the liquid phase from particle junctions it diffuses more along  
504 the nanocrystalline grains. Whereas the SPS reprocessing at 750 °C already has the intergranular Nd-rich phase in a  
505 liquid state and it begins to further wet as the liquid phase is redistributed under continuous uniaxial pressure from  
506 SPS. This short-order redistribution of the Nd-rich grain boundary phase at optimal SPS conditions is the proposed  
507 reason for the  $H_{Ci}$  higher than the starting recycled HDDR powder. Only a slight grain growth of < 100 nm on average

\* Corresponding Author.

Email: [awais.ikram@ijs.si](mailto:awais.ikram@ijs.si) (Awais Ikram)

508 from the recycled HDDR powder was identified after SPS-ing in the optimal conditions. The Nd-rich phase  
509 redistribution is effective for samples SPS-ed below the abnormal grain growth temperature of 820 °C as the liquid  
510 phase has already wetted the nanocrystalline grain boundary channels and the particle boundaries. At 850 °C the  
511 nanocrystalline grains grew to the size range of 750 – 2600 nm and in parallel, the residual grains also experience  
512 grain coarsening and grow to size larger than  $\geq 10 \mu\text{m}$ , with both processes the normal and the abnormal grain  
513 growth occurring simultaneously. Due to the abnormal grain growth kinetics at elevated temperature, the pores  
514 were observed to be isolated within the coarsened grains. These pores in larger grains create internal tension and as  
515 the grains expand in size, the microstructure might experience a localized strain from the grain boundaries and  
516 secondary phases. At this point ( $> 820 \text{ }^\circ\text{C}$ ), the localized SPS overheating (high current density and Joule's heating  
517 effect) causes the larger grains to grow at the expense of smaller nanocrystalline grains and Nd-enrichments which  
518 might generate a number of defects along the coarser grains, so the post-SPS thermal treatment may also contribute  
519 in the relaxation of the interfacial strains which increases the  $H_{\text{ci}}$  (approx. 5 – 10%) and not just to the Nd-rich phase  
520 redistribution especially for the samples SPS-ed above 820 °C. Thereby the strain in the microstructure at elevated  
521 SPS conditions can be associated with the high current density due to Joules heating, pore segregation, Ostwald  
522 ripening and secondary phases compressing the matrix grains. After the thermal treatment, the microstructure is  
523 relaxed of the strain arising from the SPS reprocessing. The observed grain growth after the thermal treatment is less  
524 than 100 – 150 nm in optimally SPS reprocessed sample at 750 °C. Upon that the SPS and thermal treatment in  
525 combination are the ideal tools to preserve the coercivity of the initial HDDR powder and therefore ideal to  
526 reprocess the recycled magnet scrap to sintered magnets. The SPS temperatures  $> 820 \text{ }^\circ\text{C}$  should be avoided as it  
527 activates the Ostwald ripening and degrades the magnetic properties.

## 528 **5. Acknowledgments**

529 The research leading to these results has received the funding from the European Community's Horizon 2020  
530 Program ([H2020/2014-2019]) under Grant Agreement no. 674973 (MSCA-ETN DEMETER). Project website:  
531 <http://etn-demeter.eu/>. This publication reflects only the authors' views, which are targeted to contribute to the  
532 betterment of the global community. The authors would also like to acknowledge the Department for  
533 Nanostructured Materials (K7 Nano) for the provision of the reprocessing facilities and Center for Electron  
534 Microscopy & Microanalysis (CEMM) for analytical scanning electron microscopy at the Jozef Stefan Institute  
535 Slovenia. We also extend our thanks on the support offered Mr. Luka Kelhar (MSc.) for the XRD analysis at JSI  
536 Slovenia.

## 537 **References**

- 538 1) Sagawa M, Fujimura S, Togawa N, Matsuura Y., "New material for permanent magnet on a base of Nd and Fe", Journal of  
539 Applied Physics, Vol. 55: 2083, (1984).
- 540 2) Croat J J, Herbst J F, Lee R W, Pinkerton F E., "Pr-Fe and Nd-Fe-based materials: A new class of high performance permanent  
541 magnets", Journal of Applied Physics, Vol. 55: 2078, (1984).

\* Corresponding Author.

Email: [awais.ikram@ijs.si](mailto:awais.ikram@ijs.si) (Awais Ikram)

- 542 3) H. R. Kirchmayr, "Permanent magnets and hard magnetic materials" *Journal of Physics D: Applied Physics*, Vol. 29, pg.  
543 2763–2778, (1996).
- 544 4) S Sugimoto, "Current status and recent topics of rare-earth permanent magnets", *Journal of Physics D: Applied Physics*, Vol.  
545 44: 064001, (2011).
- 546 5) Narayan Poudyal and J Ping Liu, "Advances in nanostructured permanent magnets research", *Journal of Physics D: Applied*  
547 *Physics*, Vol. 46: 043001, pg. 23, (2013).
- 548 6) *Critical Raw Materials for the EU*, European Commission, Brussels, Belgium, (2014).
- 549 7) Li Xiantao, Yue Ming, Zakotnik Miha, Liu Weiqiang, Zhang Dongtao, Zuo Tiejong, "Regeneration of waste sintered Nd-Fe-B  
550 magnets to fabricate anisotropic bonded magnets", *Journal of Rare Earths*, Vol. 33, No. 7, Pg. 736, (2015).
- 551 8) Gutfleisch O, Willard M A, Brück E, Chen C H, Sankar S G, Liu J P., "Magnetic materials and devices for the 21<sup>st</sup> century:  
552 stronger, lighter, and more energy efficient", *Advanced Materials*, Vol. 23: 821, (2011).
- 553 9) A. Walton, Han Yi, N.A. Rowson, J.D. Speight, V.S.J. Mann, R.S. Sheridan, A. Bradshaw, I.R. Harris, A.J. Williams", "The use of  
554 hydrogen to separate and recycle neodymium iron boron-type magnets from electronic waste", *Journal of Cleaner*  
555 *Production*, Vol. 104, pg. 236-241, (2015).
- 556 10) Li C, Liu W Q, Yue M, Liu Y Q, Zhang D T, Zuo T Y., "Waste Nd-Fe-B sintered magnet recycling by doping with rare earth rich  
557 alloys" *IEEE Transactions in Magnetism*, Vol. 50: 2105403, (2014).
- 558 11) Sprecher B, Xiao Y P, Walton A, Speight J, Harris R, Kleijn R, Visser G, Kramer G J., "Life cycle inventory of the production of  
559 rare earths and the subsequent production of NdFeB rare earth permanent magnets", *Environmental Science and*  
560 *Technology*, Vol. 48: 3951, (2014).
- 561 12) Périgo E. A., da Silva S. C., Martin R. V., Taklishi H., Landgraf F J G., "Properties of hydrogenation-disproportionation-  
562 desorption-recombination NdFeB powders prepared from recycled sintered magnets", *Journal of Applied Physics*, Vol. 111:  
563 07A725, (2012).
- 564 13) Sheridan R S, Sillitoe R, Zakotnik M, Harris I R, Williams A J., "Anisotropic powder from sintered NdFeB magnets by the HDDR  
565 processing route", *Journal of Magnetism and Magnetic Materials*, Vol. 324: 63, (2012).
- 566 14) Zakotnik M, Harris I R, Williams A J., "Possible methods of recycling Nd-Fe-B-type sintered magnets using the HD/degassing  
567 process", *Journal of Alloys Compounds*, Vol. 450: 525, (2008).
- 568 15) Zakotnik M, Harris I R, Williams A J., "Multiple recycling of NdFeB-type sintered magnets", *Journal of Alloys Compounds*, Vol.  
569 469: 314, (2009).
- 570 16) Itoh M, Masuda M, Suzuki S, Machida K., "Recycling of rare earth sintered magnets as isotropic bonded magnets by melt-  
571 spinning", *Journal of Alloys Compounds*, Vol. 374: 393, (2004).
- 572 17) Gutfleisch O, Güth K, Woodcock T G., "Recycling used Nd-Fe-B sintered magnets via a hydrogen-based route to produce  
573 anisotropic, resin bonded magnets", *Advanced Energy Materials*, Vol. 3: 151, (2013).
- 574 18) Itoh M, Masuda M, Suzuki S, Machida K., "Recycle for sludge scrap of Nd-Fe-B sintered magnet as isotropic bonded  
575 magnet", *Journal of Rare Earths*, Vol. 22: 168, (2004).
- 576 19) Kim A S, Kim D H, Namkung S, Jang T S, Lee D H, Kwon H W, Hwang D H., "Development of high coercive powder from the  
577 Nd-Fe-B sintered magnet scrap", *IEEE Transactions on Magnetism*, Vol. 40: 2877, (2004).
- 578 20) P. J. McGuinness, C. Short, A. F. Wilson, I. R. Harris, *Journal of Alloys Compounds*, Vol. 184, pg. 243–255, (1992).
- 579 21) K. H. Müller, W. Grünberger, D. Hinz, B. Gebel, D. Eckert, A. Handstein, *Materials Letters*, Vol. 34, pg. 50–54, (1998).

\* Corresponding Author.

Email: [awais.ikram@ijs.si](mailto:awais.ikram@ijs.si) (Awais Ikram)

- 580 22) K. Suresh, T. Ohkubo, Y. K. Takahashi, K. Ohishi, R. Gopalan, K. Hono, T. Nishiuchi, N. Nozawa, S. Hirosawa, "Consolidation of  
581 hydrogenation–disproportionation–desorption– recombination processed Nd–Fe–B magnets by spark plasma sintering",  
582 Journal of Magnetism and Magnetic Materials, Vol. 321, pg. 3681–3686, (2009).
- 583 23) K. Takagi, M. Akada, R. Soda, K. Ozaki, "Preparation of Nd–Fe–B sintered magnets from HDDR-processed powder", Journal  
584 of Magnetism and Magnetic Materials, Vol. 393, pg. 461–466, (2015).
- 585 24) R. Gopalan, H. Sepehri-Amin, K. Suresh, T. Ohkubo, K. Hono, T. Nishiuchi, N. Nozawa and S. Hirosawa, "Anisotropic Nd–Fe–  
586 B nanocrystalline magnets processed by spark plasma sintering and in situ hot pressing of hydrogenation–decomposition–  
587 desorption–recombination powder", Scripta Materialia, Vol. 61, pg. 978–981, (2009).
- 588 25) W. F. Li, T. Ohkubo, K. Hono, T. Nishiuchi, and S. Hirosawa, "Coercivity mechanism of hydrogenation disproportionation  
589 desorption recombination processed Nd–Fe–B based magnets", Applied Physics Letters, Vol. 93, 052505 (2008).
- 590 26) N. Nozawa, H. Sepehri-Amin, T. Ohkubo, K. Hono, T. Nishiuchi, S. Hirosawa, Journal of Magnetism and Magnetic Materials,  
591 Vol. 323, pg. 115–121, (2011).
- 592 27) H. Nakamura, K. Hirota, M. Shima, T. Minowa, and M. Honshima, "Magnetic Properties of Extremely Small Nd–Fe–B  
593 Sintered Magnets", IEEE Transactions on Magnetics, Vol. 41, No. 10, (2005).
- 594 28) H. W. Kwon, J. G. Lee and J. H. Yu, "Origin of radical coercivity reduction in fine Nd-Fe-B-type hydrogenation,  
595 disproportionation, desorption, recombination particles and its recovery", Journal of Applied Physics, Vol. 115, 17A727,  
596 (2014).
- 597 29) R. S. Sheridan, A. J. Williams, I. R. Harris, A. Walton, "Improved HDDR processing route for production of anisotropic powder  
598 from sintered NdFeB type magnets" Journal of Magnetism and Magnetic Materials, Vol. 350, pg. 114–118, (2014).
- 599 30) Hu, Z. H., Zhu, M. G., Li, W., Lian, F. Z.; "Effects of Nb on the coercivity and impact toughness of sintered Nd-Fe-B magnets."  
600 Journal of Magnetism and Magnetic Materials, Vol. 320 (3-4): 96-99, (2008).
- 601 31) Ahmed, F. M. and Harris, I. R. "Improvement of microstructure and magnetic properties of NdFeB alloys by Nb and Co  
602 additions." Journal of Magnetism and Magnetic Materials, Vol. 320: 2808-2813, (2008).
- 603 32) N. Oono, M. Sagawa, R. Kasada, H. Matsui, A. Kimura, "Production of thick high-performance sintered neodymium magnets  
604 by grain boundary diffusion treatment with dysprosium–nickel–aluminum alloy", Journal of Magnetism and Magnetic  
605 Materials, Vol. 323, pg. 297–300, (2011).
- 606 33) K. Morimoto, N. Katayama, H. Akamine, M. Itakura, "Coercivity enhancement of anisotropic Dy-free Nd–Fe–B powders by  
607 conventional HDDR process", Journal of Magnetism and Magnetic Materials, Vol. 324, pg. 3723–3726, (2012).
- 608 34) H. Sepehri-Amin, T. Ohkubo, T. Nishiuchi, S. Hirosawa, K. Hono, "Coercivity enhancement of hydrogenation–  
609 disproportionation–desorption–recombination processed Nd–Fe–B powders by the diffusion of Nd–Cu eutectic alloys",  
610 Scripta Materialia, Vol. 63, pg. 1124–1127, (2010).
- 611 35) W. F. Li, T. Ohkubo, K. Hono, T. Nishiuchi, and S. Hirosawa, "The role of grain boundaries in the coercivity of hydrogenation  
612 disproportionation desorption recombination processed Nd–Fe–B powders", Journal of Applied Physics, Vol. 105, 07A706,  
613 (2009).
- 614 36) E. Galego, H. Takiishi, R. Nunes de Faria Jr, "Magnetic Properties of Pr-Fe-Co-B Bonded HDDR Magnets with Alloying  
615 Additions", Materials Research, Vol. 10, No. 3, pg. 273-277, (2007).
- 616 37) Xiao-Qiang Li, Li Li, Ke Hu, Zhi-Cheng Chen, Sheng-Guan Qu, Chao Yang, "Microstructure and magnetic properties of  
617 anisotropic Nd–Fe–B magnets prepared by spark plasma sintering and hot deformation", Transactions of Nonferrous Metals  
618 Society of China, Vol. 24, pg. 3142–3151, (2014).

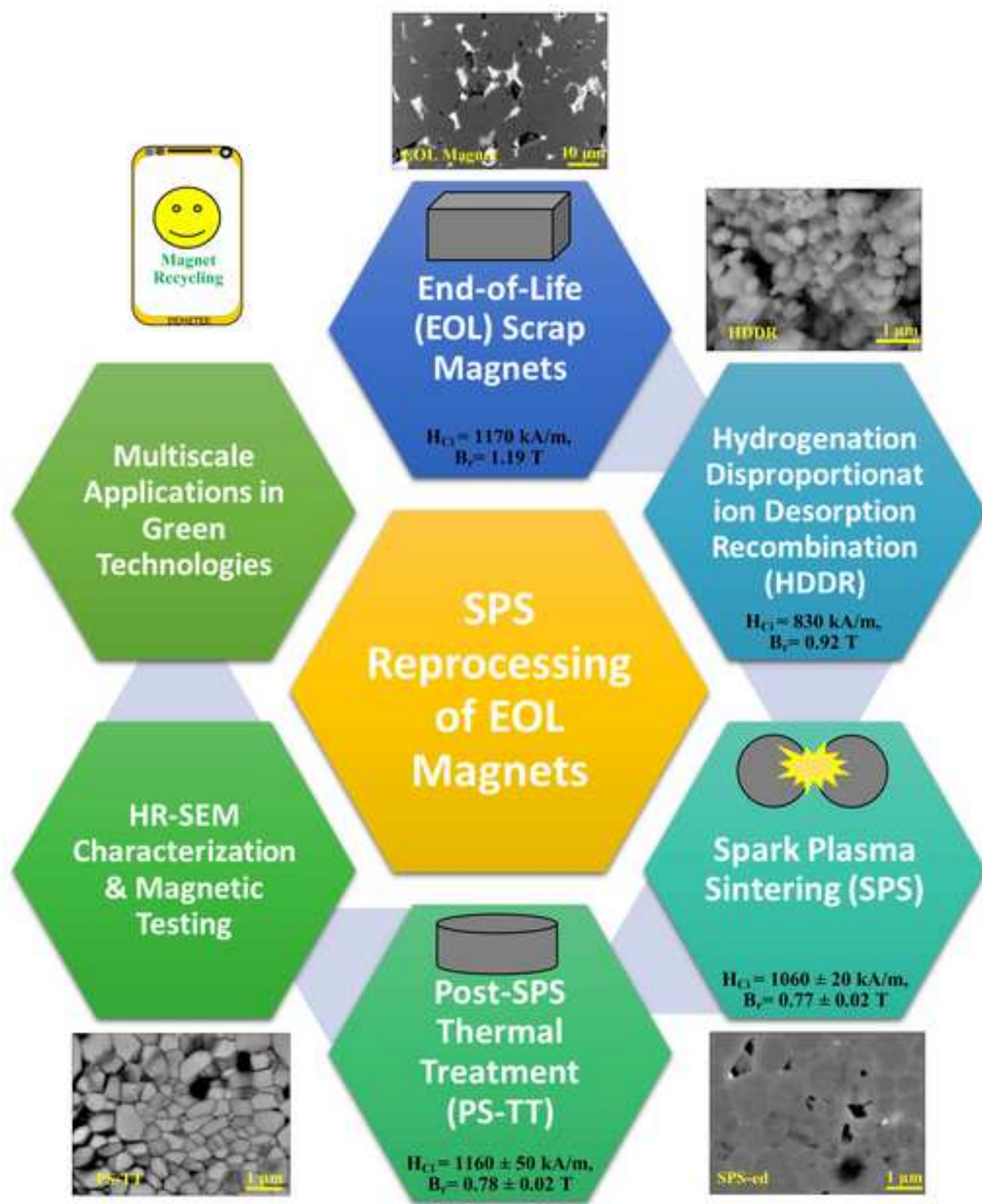
\* Corresponding Author.

Email: [awais.ikram@ijs.si](mailto:awais.ikram@ijs.si) (Awais Ikram)

- 619 38) Randall M. German, Pavan Suri, Seong Jin Park, "Review: liquid phase sintering", Journal of Materials Science, Vol. 44:1D39,  
620 (2009).
- 621 39) U.M.R. Seelam, T. Ohkubo, T. Abe, S. Hirosawa, K. Hono, "Faceted shell structure in grain boundary diffusion-processed  
622 sintered Nd-Fe-B magnets", Journal of Alloys and Compounds, Vol. 617, pg. 884-892, (2014).
- 623 40) W.F. Li, T. Ohkubo, K. Hono, "Effect of post-sinter annealing on the coercivity and microstructure of Nd-Fe-B permanent  
624 magnets", Acta Materialia, Vol. 57, pg. 1337-1346, (2009).
- 625 41) Li, W., Ohkubo, T., Akiya, T., Kato, H., & Hono, K., "The role of Cu addition in the coercivity enhancement of sintered Nd-Fe-B  
626 permanent magnets", Journal of Materials Research, Vol. 24, pg. pp. 413-420, (2009).
- 627 42) F. Vial, F. Joly, E. Nevalainen, M. Sagawa, K. Hiraga, K. T. Park "Improvement of coercivity of sintered NdFeB permanent  
628 magnets by heat treatment", Journal of Magnetism and Magnetic Materials, Vol. 242-245, pg. 1329-1334, (2002).
- 629 43) T. T. Sasaki, T. Ohkubo, K. Hono, Y. Ue, M. Sagawa, "Correlative multi-scale characterization of a fine grained Nd-Fe-B  
630 sintered magnet", Ultramicroscopy, Vol. 132, pg. 222-226, (2013).
- 631 44) W. F. Li, T. Ohkubo, K. Hono, M. Sagawa, "The origin of coercivity decrease in fine grained Nd-Fe-B sintered magnets",  
632 Journal of Magnetism and Magnetic Materials, Vol. 321, pg. 1100 - 1105, (2009).
- 633 45) M. Matsuura, R. Goto, N. Tezuka and S. Sugimoto, "Influence of Nd Oxide Phase on the Coercivity of Nd-Fe-B Thin Films",  
634 Materials Transactions, Vol. 51: 10, pg. 1901 to 1904, (2010).
- 635 46) W. Mo, L. Zhang, Q. Liu, A. Shan, J. Wu and M. Komuro, "Dependence of the crystal structure of the Nd-rich phase on  
636 oxygen content in an Nd-Fe-B sintered magnet", Scripta Materialia Vol. 59, pg. 179-182, (2008).
- 637 47) T. Fukagawa, S. Hirosawa, "Influence of Nd/Nd<sub>2</sub>Fe<sub>14</sub>B interface microstructure on the coercivity of surface Nd/Nd<sub>2</sub>Fe<sub>14</sub>B  
638 grains in Nd-sputtered Nd-Fe-B sintered magnets", Scripta Materialia, Vol. 59, pg. 183-186, (2008).
- 639 48) R. Orru, R. Licheri, A. Mario Locci, A. Cincotti, G. Cao, "Consolidation/synthesis of materials by electric current  
640 activated/assisted sintering", Materials Science and Engineering: R: Reports, Vol. 63, pg. 127-287, (2009).
- 641 49) T. Hungri, J. Galy and A. Castro, "Spark Plasma Sintering as a Useful Technique to the Nanostructuration of Piezo-  
642 Ferroelectric Materials", Advanced Engineering Materials, Vol. 11: 8, (2009).
- 643 50) Z. Zhang, Z. Liu, J. Lu, X. Shen, F. Wang and Y. Wang, "The sintering mechanism in spark plasma sintering - Proof of the  
644 occurrence of spark discharge", Scripta Materialia, Vol. 81, pg. 56-59, (2014).
- 645 51) M. N. Rahaman, Ceramic Processing and Sintering, 2nd Edition, Marcel Dekker Inc, NY, USA, (2003).
- 646 52) R. S. Sheridan, I.R. Harris, A. Walton, "The development of microstructure during hydrogenation-disproportionation-  
647 desorption-recombination treatment of sintered neodymium-iron-boron-type magnets", Journal of Magnetism and  
648 Magnetic Materials, Vol. 401, pg. 455-462, (2016).

\* Corresponding Author.

Email: [awais.ikram@ijs.si](mailto:awais.ikram@ijs.si) (Awais Ikram)



The direct recycling route for EOL scrap magnets by SPS reprocessing —100% recovery of coercivity is possible. This scheme can contribute in controlling the rare earth elements circular economy and scrap magnetic waste management.

## Highlights

- Scrap magnets are HDDR and SPS reprocessed to achieve high coercivity.
- At 4760 ppm oxygen content, the recycled HDDR powder does not lose sinterability.
- Coercivity of optimally SPS-ed HDDR powder equivalent to commercial HDDR powder.
- Coercivity after SPS reprocessing is 30% higher than starting recycled HDDR powder.
- Microstructure evolution detailed on SPS and thermally treated reprocessed powder.